1   Full title:

2   Guanosine-specific single-stranded ribonuclease effectors of a phytopathogenic fungus

3   potentiate host immune responses

4

5   Authors:

6   Naoyoshi Kumakura[1], Suthitar Singkaravanit-Ogawa[2], Pamela Gan[1], Ayako

7   Tsushima[1,6], Nobuaki Ishihama[1], Shunsuke Watanabe[1], Mitsunori Seo[1], Shintaro

8   Iwasaki[3,4], Mari Narusaka[5], Yoshihiro Narusaka[5], Yoshitaka Takano[2], Ken Shirasu[1,6*]

9

10   Affiliations:

11   [1] RIKEN Center for Sustainable Resource Science, Kanagawa, Japan

12   [2] Graduate School of Agriculture, Kyoto University, Kyoto, Japan

13   [3] RIKEN Cluster for Pioneering Research, Saitama, Japan

14   [4] Graduate School of Frontier Sciences, The University of Tokyo, Chiba, Japan

15   [5] Okayama Prefectural Technology Center for Agriculture, Forestry, and Fisheries,

16   Research Institute for Biological Sciences, Okayama, Japan

17   [6] Graduate School of Science, The University of Tokyo, Tokyo, Japan

18

19   *Corresponding author:

20   Ken Shirasu

21   Telephone: +81-45-503-9574

22   E-mail: ken.shirasu@riken.jp

23

24

Summary

Plants activate immunity upon recognition of pathogen-associated molecular patterns. Although phytopathogens have evolved a set of effector proteins to counteract plant immunity, some effectors are perceived by hosts and induce immune responses. Here, we show that two secreted ribonuclease effectors, SRN1 and SRN2, encoded in a phytopathogenic fungus, *Colletotrichum orbiculare*, induce cell death in a signal peptide- and catalytic residue-dependent manner, when transiently expressed in *Nicotiana benthamiana*. The pervasive presence of *SRN* genes across *Colletotrichum* species suggested the conserved roles. Using a transient gene expression system in cucumber (*Cucumis sativus*), an original host of *C. orbiculare,* we show that SRN1 and SRN2 potentiate host pattern-triggered immunity. Consistent with this, *C. orbiculare* SRN1 and SRN2 deletion mutants exhibited increased virulence on the host. In vitro analysis revealed that SRN1 specifically cleaves single-stranded RNAs at guanosine, leaving a 3′-end phosphate. This activity has not been reported in plants. Importantly, the potentiation of *C. sativus* responses by SRN1 and SRN2 depends on the signal peptide and ribonuclease catalytic residues, suggesting that secreted SRNs cleave RNAs in apoplast and are detected by the host. We propose that the pathogen-derived apoplastic guanosine-specific single-stranded endoribonucleases lead to immunity potentiation in plants.

Key words: *Colletotrichum orbiculare*, effector, ribonuclease, plant immunity, pathogen-associated molecular pattern (PAMP), pattern-triggered immunity (PTI)

Introduction

Plants and phytopathogens have developed mutual attack and defense systems over millions of years of coevolution. Plants are able to recognize pathogens through cell surface-localized pattern recognition receptors (PRRs). PRRs are able to perceive broadly conserved pathogen-associated molecular patterns (PAMPs), as well as damage-associated molecular patterns (DAMPs) that are host plant-derived molecules generated during pathogen invasion or cell damage. PAMPs and DAMPs include proteins, lipids, carbohydrates, and nucleic acids. Direct or indirect PAMPs/DAMPs

56   perception by PRRs induce pattern triggered-immunity (PTI), which includes both local

57   and systemic immune responses (Boutrot & Zipfel, 2017).

58   To counteract plant immune systems, pathogens have evolved secreted proteins,

59   referred to as effectors, that inhibit host immune responses and allow pathogens to

60   establish infection (Win *et al.*, 2012). However, some effectors or their functions are

61   recognized by host PRRs and induce immune responses. For example, the presence of

62   Avr2, an effector protein of *Cladosporium fluvum*, is indirectly recognized by Cf-2, a

63   PRR of tomato, and induces an immune response. Avr2 is secreted out from *C. fluvum*

64   into the host apoplastic region, binds to Rcr3, a host plant-derived protease, and inhibits

65   its enzymatic activity. Tomato indirectly senses Avr2 probably by detecting the

66   modification of Rcr3 via Cf-2 and induces an immune response to inhibit *C. fluvum*

67   infection (Dixon *et al.*, 2000; Rooney *et al.*, 2005; Tang *et al.*, 2017). Thus, effectors

68   can cause both positive and negative effects on the establishment of infection. However,

69   the mechanistic diversity of effector recognition by host PRRs is largely unknown.

70   *Colletotrichum* species are fungal pathogens that cause anthracnose disease on

71   a variety of plants including economically important crops, fruits, and vegetables (Dean

72   *et al.*, 2012; Cannon *et al.*, 2012). Most *Colletotrichum* species adopt a hemibiotroph

73   lifestyle, consisting of an early biotrophic phase with no visible symptoms and a later

74   necrotrophic phase associated with host cell death. Due to the agricultural and scientific

75   importance of *Colletotrichum* species, genome sequencing of these fungi has been

76   performed (O'Connell *et al.*, 2012; Gan *et al.*, 2013, 2016, 2021; Baroncelli *et al.*, 2014,

77   2016; Hacquard *et al.*, 2016; Tsushima *et al.*, 2019).

78   Several *Colletotrichum* effectors have been identified. For example, NIS1

79   from *Colletotrichum orbiculare*, a causal agent of Cucurbitaceae anthracnose disease,

80   suppresses PTI by inhibiting plant immunity-related kinases (Yoshino *et al.*, 2012;

81   Irieda *et al.*, 2019). For other instances, the homologous effectors CoDN3 from *C.*

82   *orbiculare* and ChEC3 from *Colletotrichum higginsianum*, a pathogen that causes

83   anthracnose disease on Brassicaceae plants, suppress plant cell death induced by NIS1

84   and NLP1, respectively, when they are expressed together in *N. benthamiana* (Yoshino

85   *et al.*, 2012; Kleemann *et al.*, 2012). Recently, a highly conserved *Colletotrichum*

86   effector candidate that induces host nuclear expansion and cell death was identified

3

87   (Tsushima *et al.*, 2021). However, *Colletotrichum* effectors such that induce an immune

88   response in the host plant have not been reported.

89   Recently, there has been an increasing number of reports on RNAs in the

90   apoplast, an interface of plant-fungal interactions. In *Arabidopsis thaliana*, apoplastic

91   fluid contains diverse small and long-noncoding RNAs (Baldrich *et al.*, 2019; Karimi *et*

92   *al.*, 2021). In addition, small RNAs are exchanged between host plants and colonizing

93   organisms, such as parasitic plants or microbes (Weiberg *et al.*, 2013; Wang *et al.*,

94   2016; Zhang *et al.*, 2016; Shahid *et al.*, 2018; Cai *et al.*, 2018). Thus, apoplast may

95   serve a place of communications between the different organisms. However, the nature

96   and roles of RNAs in the apoplast in plant-microbe interactions are still open questions.

97   Here, we show that *C. orbiculare* ribonuclease effectors potentiate host

98   immune responses in their catalytic residue-dependent manner. By comparing the

99   genomes of two different *Colletotrichum* species, we identified 21 conserved effector

100 candidates that are expressed upon infection. Among these, secreted ribonuclease 1

101 (SRN1) and the close homolog SRN2 were found as cell death-inducing effectors when

102 transiently expressed in *N. benthamiana*. Interestingly, however, neither SRN1 nor

103 SRN2 induced cell death in *Cucumis sativus*, an original host of *C. orbiculare* from

104 which the strain was isolated. Instead, SRN1 and SRN2 potentiated host immune

105 responses; *C. orbiculare srn1 srn2* double deletion mutants showed increased virulence

106 on *C. sativus*. Importantly, the potentiation of host immunity requires ribonuclease

107 catalytic residues as well as the signal peptide, implying that SRNs cleave RNAs in the

108 apoplast and are detected by the host. Consistent with this scenario, biochemical

109 analysis revealed that SRN1 is a single-stranded RNA (ssRNA) specific ribonuclease,

110 cleaving at guanosine and leaving a 3′-end phosphate. Collectively, our data suggest

111 that the enzymatic nature of SRN1 secreted from a phytopathogenic fungus can be

112 recognized by the host cell to drive plant immunity. Our study reveals a novel aspect of

113 plant-microbe interaction mediated by specific single-stranded ribonuclease effectors.

114

115 **Materials and Methods**

116 **Identification of conserved effector candidates**

117 Conserved effector candidates among *C. orbiculare* and *C. higginsianum* were

118 identified as described in Fig. 1a. Orthologs of *C. orbiculare* secreted proteins were

119 identified in *C. higginsianum* (O'Connell *et al.*, 2012) by performing a BLASTp search

120 (E-value cut-off 1E-9). Hits were further filtered by searching for evidence of

121 expression in *C. higginsianum* orthologs according to expression sequence tag (EST)

122 data (Takahara *et al.*, 2009), removing hits that were annotated with the keywords

123 glycosylphosphatidylinositol (GPI), membrane, mitochondrial or cytochrome, and

124 retaining sequences that encoded proteins of less than 350 amino acids. To identify

125 genes with potential roles in infection, only the highest scoring BLASTp hits of *C.*

126 *orbiculare* genes that had previously been shown to be up-regulated *in planta* (Gan *et*

127 *al.*, 2013) were selected (Supporting Information Table S1).

128

129 **Identification of PF00545 ribonucleases from diverse fungi**

130 Hmmscan was run against the Pfam 27.0 database using the default settings to identify

131 proteins with the PF00545 ribonuclease domain (Finn *et al.*, 2014; Eddy, 2011).

132 Searches were run against 32 genomes from diverse fungi (Supporting Information

133 Table S2) (Goffeau *et al.*, 1996; Galagan *et al.*, 2003; Loftus *et al.*, 2005; Dean *et al.*,

134 2005; Kämper *et al.*, 2006; Cuomo *et al.*, 2007; Espagne *et al.*, 2008; Coleman *et al.*,

135 2009; Martin *et al.*, 2010; Spanu *et al.*, 2010; Rouxel *et al.*, 2011; Kubicek *et al.*, 2011;

136 Duplessis *et al.*, 2011; Goodwin *et al.*, 2011; Klosterman *et al.*, 2011; Amselem *et al.*,

137 2011; Yang *et al.*, 2011; Berka *et al.*, 2011; Arnaud *et al.*, 2012; O'Connell *et al.*, 2012;

138 Gan *et al.*, 2013, 2016, 2017; Blanco-Ulate *et al.*, 2013; Cissé *et al.*, 2013; Tisserant *et*

139 *al.*, 2013; Baroncelli *et al.*, 2014; Hu *et al.*, 2014; Gazis *et al.*, 2016; Zampounis *et al.*,

140 2016).

141 Proteins identified with the PF00545 domain were aligned by MAFFT and

142 trimmed using trimAl (Katoh *et al.*, 2002; Capella-Gutiérrez *et al.*, 2009) using the

143 default automated settings in both programs. The trimmed alignment was then used to

144 construct a maximum likelihood tree with RAxML using the PROTAUTOGAMMA

145 setting and 1,000 bootstrap replicates (Stamatakis, 2006). The conservation of active

146 sites was assessed by checking for residues corresponding to *Aspergillus oryzae*

147 ribonuclease T1 (RNase T1) Y64, H66, E84, R103, and H118 in the conserved domain

148 cd00606 (NCBI's conserved domain database) (Marchler-Bauer *et al.*, 2017).

149 To generate the fungal species phylogenetic tree, single copy gene families

150 were identified by orthoMCL (Li *et al.*, 2003) from the 32 fungi analyzed using

151   all-vs-all BLASTp with a cut-off E-value of 1E-5 and an inflation value of 1.5.

152   Sequences from individual gene families were aligned using MAFFT and trimmed

153   using trimAl (Katoh *et al.*, 2002; Capella-Gutiérrez *et al.*, 2009) as described above.

154   Then, trimmed alignments from the 501 single copy gene families identified were

155   concatenated resulting in a dataset of 227,412 sites. The concatenated alignment was

156   used for RAxML analysis which was carried out as described above. *Rhizophagus*

157   *irregularis* was set as the root using FigTree v1.4.2 (Rambaut, Andrew) in the best

158   estimated tree, which was then converted to an ultrametric chronogram using r8s

159   version 1.8 (Sanderson, 2003) using the Langley-Fitch molecular clock model.

160   Previously estimated divergence times of 443–695 million years ago (mya) for

161   Pezizomycotina-Saccharomycotina, 400-583 mya for the Pezizomycotina crown group,

162   267-430 mya for the Leotiomycetes-Sordariomycetes, 207-339 mya for

163   Sordariomycetes, 487-773 mya for the Ascomycete crown (Beimforde *et al.*, 2014) and

164   47 mya for the divergence between *C. graminicola* and *C. higginsianum* (O'Connell *et*

165   *al.*, 2012) were used to calibrate the tree. The phylogenetic trees generated were

166   visualized in the interactive Tree of Life (Letunic & Bork, 2016).

167

168   **Prediction of SRN homologs in 22 *Colletotrichum* species**

169   Using amino acid sequences of *C. orbiculare* SRN1, SRN2, SRN3.1, SRN3.2, and

170   SRN4 as queries, genomes of 22 *Colletotrichum* species were searched by Exonerate

171   version 2.2 software. Proteins lacking signal peptides predicted by SignalP 4.1 software

172   (Petersen *et al.*, 2011) were removed. The sequences were aligned using Molecular

173   Evolutionary Genetics Analysis (Mega) Version 7.0 (Kumar *et al.*, 2016). The

174   phylogenetic tree of the SRN homologs was then drawn using the same software.

175

176   **Plant growth conditions**

177   *N. benthamiana* plants were grown in a mixture of equal amounts of Supermix A

178   (Sakata Seed Corp.) and vermiculite in 8 cm TO poly-pots (Tokai Agri System) under

179   16 h light:8 h dark conditions at 25 ˚C. *C. sativus* strain Suyo (Sakata Seed Corp.)

180   plants were grown in the same soil mix and incubated under 10 h light: 14 h dark

181   conditions at 24 ˚C.

182

Plasmids

Plasmids used in this study are listed in Supporting Information Table S3. The method for plasmid construction is described in Supporting Information Method S1. Primers used in this study are listed in Supporting Information Table S4.

Transient gene expression in *N. benthamiana* and *C. sativus*

Agrobacterium-mediated transient gene expression was performed following the previously described method with modifications (Chen *et al.*, 2021). The *Agrobacterium tumefaciens* GV3101 and GV2260 strains were used. GV2260 strains were transformed with both pBBR*gabT* (Nonaka *et al.*, 2017) and pEAQ-based plasmids (Sainsbury *et al.*, 2009). The *Agrobacterium* culture was washed and resuspended in infiltration solution (10 mM MES pH 5.6, 10 mM $MgCl_2$, and 150 μM acetosyringone). Infiltration solutions were at a density of O.D. 600 = 0.3. Each infiltration solution was infiltrated into 4-5 week-old *N. benthamiana* leaves or 6-9 day-old cotyledons of *C. sativus* using 1 ml syringes (TERUMO). An ultraviolet lamp MODEL B-100AP (UVP) was used for UV illumination. Photographs were taken using an EOS Kiss X6i (Canon). For UV illuminated leaves, a Y2 Professional Multi Coated Camera Lens Filter (Kenko) was used.

RNA isolation, cDNA synthesis, and RT-qPCR

For obtaining vegetative hyphae (VH), *C. orbiculare* wild-type strain 104-T (MAFF 240422) was cultured on potato dextrose agar (PDA) medium (Nissui) then transferred onto potato dextrose (BD) liquid media and incubated for 3 days at 25 ˚C in the dark. For obtaining conidia, *C. orbiculare* hyphae were inoculated onto PDA media and incubated at 25 ˚C under black light blue light (10 h light: 14 h dark) for 6 days. Conidia were then suspended in water, filtered and collected by centrifugation. For one, three, and seven days post-inoculation (dpi), 1×10^6 conidia ml^{-1} *C. orbiculare* conidia in 0.02% Silwet L-77 (Bio Medical Science) were inoculated onto the abaxial side of *C. sativus* cotyledons at 10 days post-germination (dpg) using a brush. Peeled epidermal cells were used for 1 and 3 dpi samples. Whole leaf tissues were used for 7 dpi samples. Three independent biological replicates were prepared for each sample.

214   For fungal biomass measurements, leaf disks were collected from *C. sativus*

215   cotyledons infected with fungi at 88 hours post-inoculation (hpi) (as described in Fungal

216   inoculation section) using a cork borer (4 mm diameter). Each sample consisted of at

217   least six leaf disks from at least six leaves. Six replicates were prepared for each sample.

218   All samples were transferred into 2-ml steel-top tubes, frozen using liquid nitrogen, and

219   stored at -80 ˚C until RNA isolation. Total RNA isolation, DNA removal, cDNA

220   synthesis and real-time quantitative PCR (RT-qPCR) reactions were performed as

221   previously described (Kumakura *et al.*, 2019) with slight modifications. First strand

222   cDNA synthesis was performed with the ReverTra Ace qPCR RT Kit (TOYOBO) using

223   the included primer mix, as well as gene-specific primers (listed in Supporting

224   Information Table S4). Primer pairs used for RT-qPCR are also listed in Supporting

225   Information Table S4.

226

227   Fungal transformation and inoculation

228   The methods for fungal transformation and fungal inoculation are described in

229   Supporting Information Method S2 and S3, respectively.

230

231   Sequence alignment of SRNs

232   Amino acid sequences were aligned using CLC Genomics Workbench8 (CLC Bio). All

233   coding sequences of *C. orbiculare* SRNs used in this report were cloned from *C.*

234   *orbiculare* cDNAs and sequenced for verification.

235

236   Measurement of oxidative burst from leaf disks

237   To detect chitin-induced reactive oxygen species (ROS) bursts, eight leaf disks were

238   collected from *C. sativus* leaves using a cork borer (4 mm diameter) (Kai industries Co.,

239   Ltd.). Leaf disks were floated for more than 10 h on sterile water in 96-well microplates

240   (655075, Greiner Bio-One), then the water was substituted by a solution containing 10

241   mg ml^{-1} horseradish peroxidase (Sigma), 1 μM L-012 (Wako), and 10 μM chitin

242   heptose (Oligo Tech). Luminescence was measured for 30 min using a TriStar2 LB942

243   multi-plate reader (Berthold) (Kadota *et al.*, 2018).

244

245   Immunoblotting

246   The method for immunoblotting is described in Supporting Information Method S4.

247

248   **Protein deglycosylation enzyme treatment**

249   Proteins isolated from *N. benthamiana* using the method described in the

250   immunoblotting section were treated with Protein Deglycosylation Mix II (New

251   England BioLabs) following the manufacturer's protocol. Then, Samples were mixed

252   with SDS-Laemmli buffer and analyzed by immunoblot.

253

254   **Recombinant protein expression and purification**

255   The method for immunoblotting is described in Supporting Information Method S5.

256

257   **In vitro RNase assay**

258   RNA substrates used in this study are shown in Fig. 6a, 6b, and Supplementary

259   Information Fig. S7c. As ssRNA substrates, AG10

260   (5′-AGAGAGAGAGAGAGAGAGAG-3′), UC10

261   (5′-UCUCUCUCUCUCUCUCUCUC-3′), ssRNA1

262   (5′-AUCAUGCAUCAUCAUCAUCA-3′), ssRNA2

263   (5′-AUCAUCAUCAGUCAUCAUCA-3′), ssRNA3

264   (5′-AUCAUCAUCAUCAUCGAUCA-3′), ssRNA4

265   (5′-UCGCGUUGAUUACCCUGUUAUCCCUAGUGUACAU-3′) were chemically

266   synthesized with fluorescein (FAM) addition at their 5′ end by Hokkaido System

267   Science Co., Ltd. As a double-stranded RNA (dsRNA) substrate, dsRNA4 was prepared

268   as following. ssRNA4 and chemically synthesized ssRNA

269   (5′-AUGUACACUAGGGAUAACAGGGUAAUCAACGCGA-3′) which is

270   complementary to ssRNA4 were mixed in buffer (20 mM Tris-HCl pH7.5, 150 mM

271   NaCl, 1 mM DTT, and 2 mM $MgCl_2$). The mixture was incubated at 95 °C for 5 min

272   and then at room temperature for 30 min, resulting in dsRNA4.

273   For in vitro RNase assay, recombinant proteins or commercially available

274   RNase T1 (Thermo Fisher Scientific) were mixed with 0.5 pmol substrate RNAs in 10

275   µl RNase reaction buffer with EDTA (20 mM Tris-HCl pH7.5, 150 mM NaCl, 1 mM

276   DTT, and 5 mM EDTA) or 10 µl RNase reaction buffer with $MgCl_2$ (20 mM Tris-HCl

277   pH7.5, 150 mM NaCl, 1 mM DTT, and 5 mM $MgCl_2$). The reaction was incubated for

9

278   30 min at 25 ˚C, then mixed with an equal volume of 2×RNA loading buffer [95% (v

279   v^{-1}) formamide, 0.025% (w v^{-1}) SDS, and 0.5 mM EDTA], incubated 95 ˚C for 3 min,

280   and cooled on ice for 1 min. The reaction was separated by 15% denaturing acrylamide

281   urea gel electrophoresis. Signals of FAM labelled RNAs were detected using PharosFX

282   (Bio-Rad) imaging systems.

283

284   **Linker ligation of RNAs**

285   Linker ligation of RNAs was performed as previously described (Mito *et al.*, 2020).

286   Details are in Supporting Information Method S6.

287

288   **Results**

289   **Prediction of *Colletotrichum* conserved effectors and identification of a cell**

290   **death-inducing effector in *N. benthamiana***

291   To survey conserved effectors in the *Colletotrichum* genus, we reasoned that the

292   candidates should be secreted to interact with host plant, conserved in the genus, and

293   highly expressed during infection. Considering these criteria, we compared protein

294   sequences from *C. orbiculare* and *C. higginsianum*, belonging to the orbiculare and

295   destructivum species complexes, respectively. A total of 21 small secreted orthologous

296   proteins, with evidence of up-regulation both in *C. higginsianum* and *C. orbiculare*

297   during infection (Takahara *et al.*, 2009; Gan *et al.*, 2013), were selected as effector

298   candidates conserved in the two pathogens (Fig. 1a, Supporting Information Table S1).

299   Among them, we found that one of the *C. orbiculare* effector

300   candidates induced cell death (Fig. 1b) when expressed transiently in *N. benthamiana.*

301   The gene that induced cell death (Locus tag: Cob_v010174) was named *SECRETED*

302   *RIBONUCLEASE 1* (*SRN1*), due to the presence of the ribonuclease domain (Pfam

303   database: PF00545, NCBI's conserved domain database: cd00606) and the signal peptide

304   sequence (Fig. 1c). The *C. orbiculare* genome is predicted to encode three other

305   *SRN1*-like genes and we therefore termed them as *SRN2*, *SRN3* and *SRN4* (Supporting

306   Information Fig. S1a, Table S6). By cloning the coding sequences from the cDNA of *C.*

307   *orbiculare* we found that each gene transcript had a single isoform except for *SRN3*,

308   which had two different isoforms (denoted as *SRN3.1* and *SRN3.2*) (Fig. 1c).
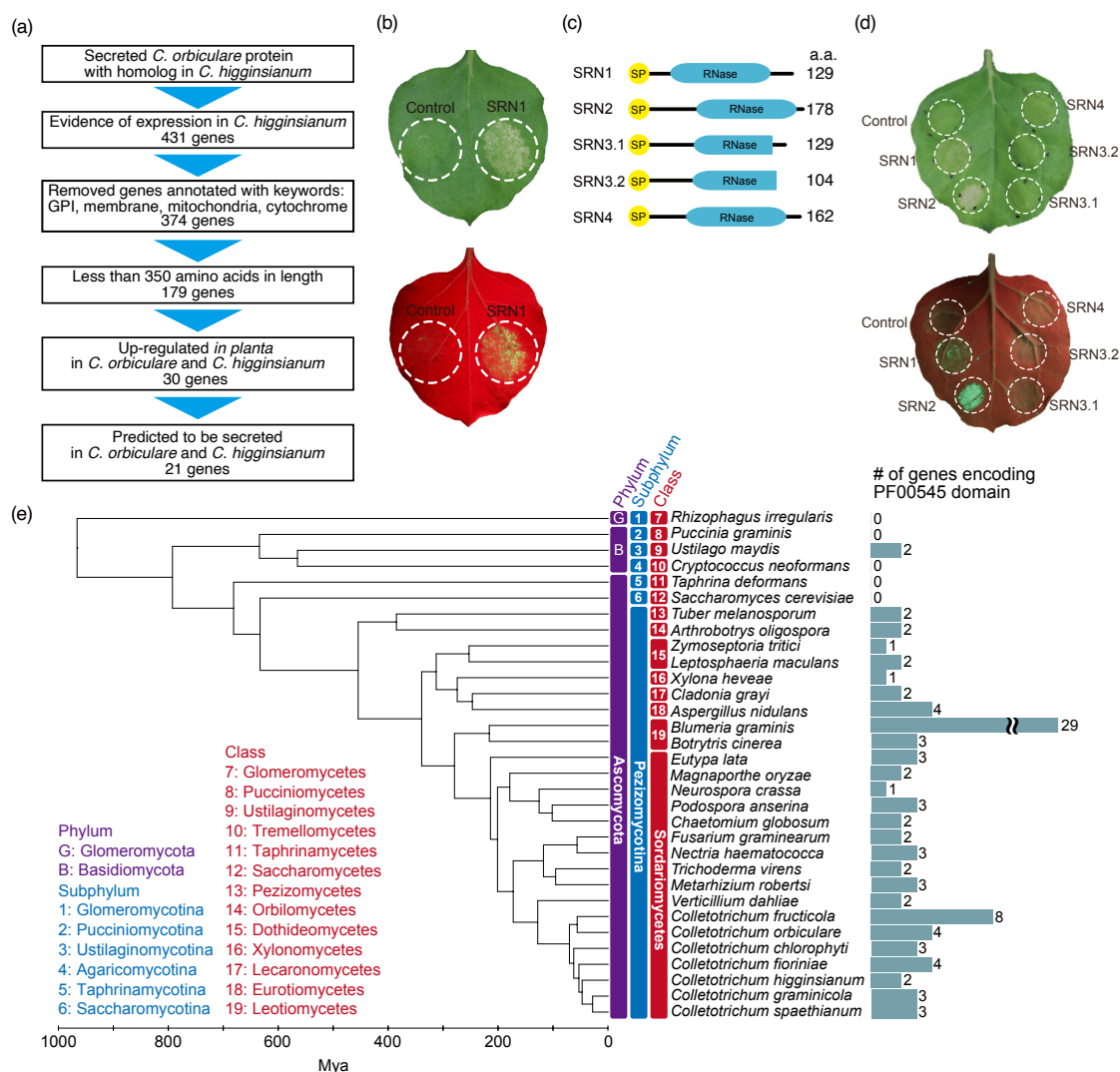
Figure 1. Identification of conserved *Colletotrichum* effectors that induce cell death in *N. benthamiana*

(a) Effector prediction pipeline in *C. orbiculare* and *C. higginsianum*. (b) *N. benthamiana* leaf expressing *C. orbiculare SRN1* using the *Agrobacterium*-mediated transient gene expression system. The pGWB2 binary vector was used. An *Agrobacterium* strain transformed with an empty vector was used for control. Photographs were taken at 6 days post-inoculation (dpi). The bottom image was taken under ultraviolet illumination to visualize plant cell death in green with autofluorescence. (c) Schematics of *C. orbiculare* SRN proteins. Yellow and blue boxes represent the signal peptides and RNase domains, respectively, that are conserved among SRN homologs. a. a. represents number of amino acids. (d) Cell death phenotypes of SRN1, SRN2, SRN3.1, SRN3.2, and SRN4 expressed as in (b). (e) PF00545 ribonuclease domain-containing proteins are highly conserved in fungi. Numbers of PF00545 ribonuclease domain-containing proteins in different fungi. Divergence dates were estimated based on a maximum likelihood tree constructed from 501 single copy genes in all the analyzed fungi using the program r8s.

11

326 SRN1, SRN2, and SRN4 had five conserved ribonuclease catalytic residues inside their

327 ribonuclease domains, while SRN3.1 and SRN3.2 contained only the first three

328 (Supporting Information Fig. S1b) (Nishikawa *et al.*, 1987; Noguchi *et al.*, 1995;

329 Marchler-Bauer *et al.*, 2017).

330 To test the functional resemblance with *SRN1*, cell death induced by *SRN2*,

331 *SRN3.1*, *SRN3.2*, and *SRN4* expressions was monitored in *N. benthamiana*. Like *SRN1*,

332 *SRN2* induced cell death, while *SRN3.1*, *SRN3.2* and *SRN4* did not (Fig. 1d). Since the

333 insufficient expression may hamper the conclusion, we harnessed the pEAQ-HT vector,

334 which enables higher expression of proteins (Sainsbury *et al.*, 2009). In this system, in

335 addition to *SRN1* and *SRN2*, *SRN4* also induced cell death in *N. benthamiana*

336 (Supporting Information Fig. S2a). The proteins with C-terminal HA tag did not impact

337 on the cell death induced by *SRN1*, *SRN2*, and *SRN4* (Supporting Information Fig. S2b).

338 We note that *SRN3.1-HA* weakly induced cell death in this high-expression system,

339 while *SRN3.2-HA* did not, despite its expression being confirmed by immunoblot

340 analysis (Supporting Information Fig. S2c).

341

342 ***SRN* homologs are conserved in all 22 *Colletotrichum* species tested**

343 To analyze the conservation of *SRN1*, we surveyed the PF00545 ribonuclease domain in

344 the Pfam database (Finn *et al.*, 2014) because *SRN1* encodes the domain. Genes

345 encoding PF00545 domains were conserved in bacteria and fungi, especially in

346 Ascomycota, but not in plants and animals (Pfam 34.0) (Mistry *et al.*, 2021) (Fig. 1e, 2),

347 suggesting that PF00545 is the microorganisms specific domain. In fungi, all 26

348 Pezizomycotina species tested were predicted to encode proteins with the PF00545

349 domain. However, most species belonging to the Glomeromycota and Basidiomycota

350 did not have the PF00545 domain, except for *Ustilago maydis*, a causal agent of corn

351 smut.

352 To confirm if SRNs are conserved in the *Colletotrichum* genus, the genomes

353 of 22 available *Colletotrichum* species (Supporting Information Table S7) were

354 surveyed for the presence of SRN homolog-encoding sequences. Full-length amino acid

355 sequences of *C. orbiculare* SRN1, SRN2, SRN3.1, SRN3.2, and SRN4 were used to

356 query the whole genome sequences of the 22 species. All species tested had at least two

357 SRN homologs (Supporting Information Table S7).

12
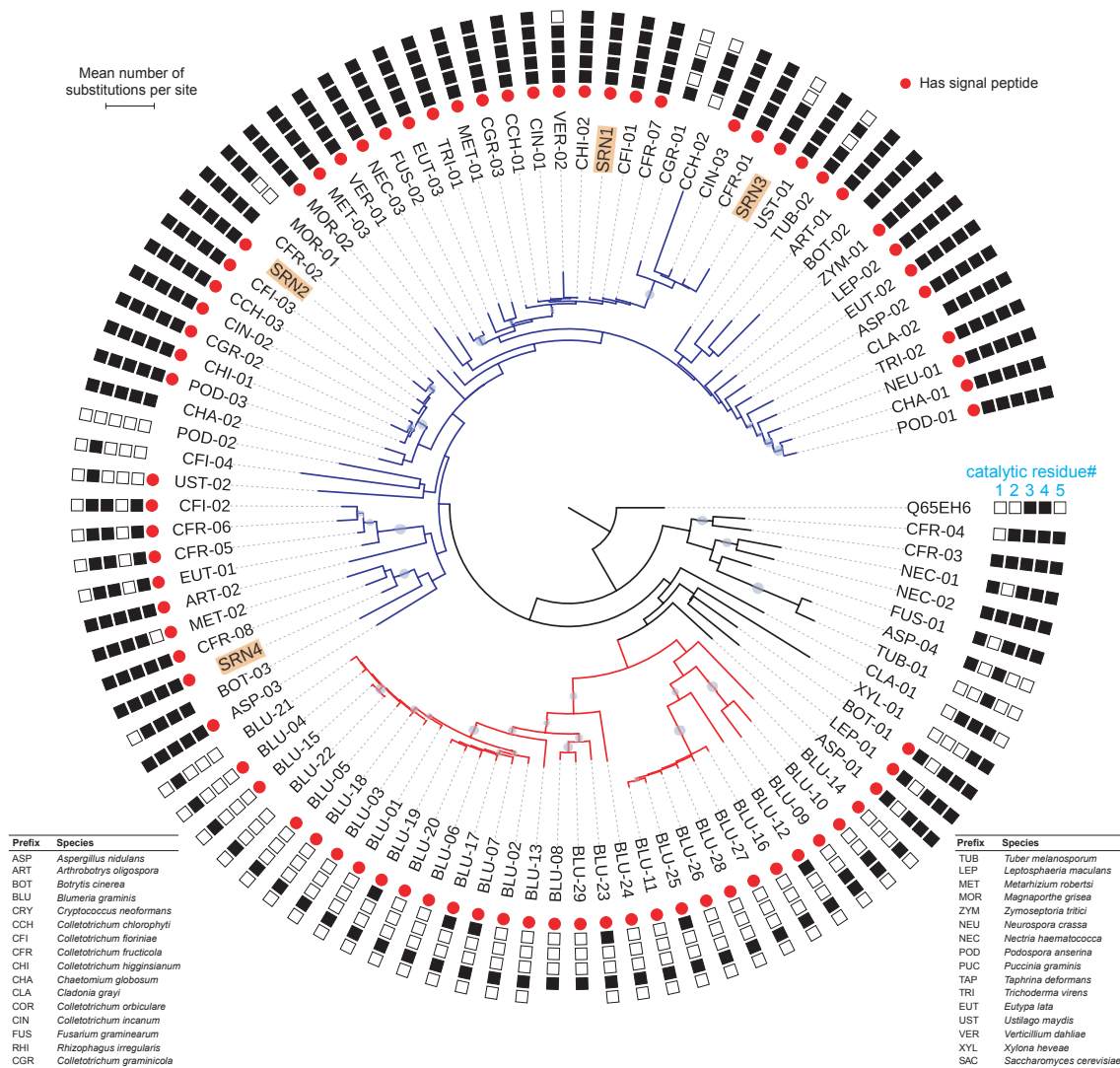
Figure 2. Phylogenetic relationship between fungal ribonuclease proteins
Maximum likelihood tree of sequences associated with the PF00545 ribonuclease domain in 32 different fungi drawn using the RAxML software. Grey circles on branches indicate branches with more than 50% bootstrap support values out of 1000 replicates. Black squares indicate conservation of five residues that are important for the ribonuclease catalytic activity. Red circles indicate the presence of a signal peptide according to the analysis by SignalP4.0.

368   Based on the sequence similarity, the SRN homologs were classified into three groups
369   named SRN1/3, SRN2, and SRN4. All 22 species had homologs belonging to the
370   SRN1/3 and SRN2 groups, but only species from the gloeosporioides and orbiculare
371   species complexes had the SRN4 group genes (Supporting Information Table S7). All
372   species from the same species complex had the same composition of SRN homologs,
373   except for the spaethianum species complex (Supporting Information Table S7).

374

375   **Cell death by *SRNs* is not observed in *C. sativus*, an original host of *C. orbiculare***
376   The SRN-mediated cell death observed in *N. benthamiana* led us to test the same
377   phenotype in *C. sativus* (cucumber), an original host of *C. orbiculare*. To set out the
378   protein expression in cucumber, we applied an *Agrobacterium*-mediated transient gene
379   expression system established in melon (Chen *et al.*, 2021) with several modifications.
380   Here we used *A. tumefaciens* GV2260 strain which has the enhanced T-DNA
381   translocation activity in certain plant species through expressing *gabT* gene (Nonaka *et*
382   *al.*, 2017). Indeed, this system allowed to accumulate GFP protein (as a marker protein)
383   in fluorescence imaging (Supporting Information Fig. S3a) and in immunoblot
384   (Supporting Information Fig. S3b). Harnessing this setup, we expressed *C. orbicualre*
385   SRNs in *C. sativus*. Contrary to our expectation by *N. benthamiana* experiments, none
386   of the *SRN* constructs induced detectable cell death on *C. sativus* cotyledons despite the
387   detection of protein expression from these constructs (Fig. 3a, b).

388

389   **SRN1 and SRN2 enhance chitin-triggered ROS bursts in *C. sativus***
390   Given the tolerance to ectopic SRN expression in *C. sativus*, we were intrigued by the
391   *SRN* genes expression profiles during *C. orbiculare* infection. RT-qPCR analysis
392   revealed that all *SRNs*, except for SRN3.1 and SRN3.2, were strongly induced during
393   infection compared to VH, non-inoculated fungal cells, especially at 1 dpi (Fig. 3c),
394   implying that these effectors are likely to be involved in plant-fungi interaction at the
395   early biotrophic phase. The upregulation of *SRNs* at 1 dpi prompted us to test if *SRNs*
396   impact on plant immune responses in *C. sativus*. For this purpose, we monitored ROS
397   bursts, a typical PTI response, triggered by chitin treatment (Torres *et al.*, 2006). As
398   shown in Supporting Information Fig. S4, chitin treatment strongly induced ROS bursts
399   in *C. sativus* cotyledons.
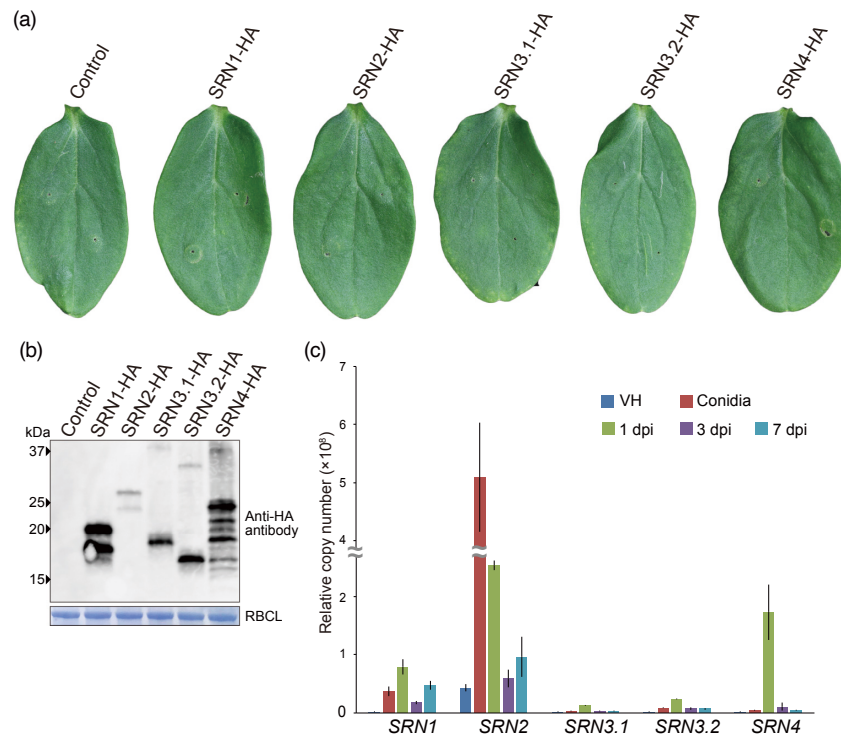
Figure 3. Expression of *C. orbiculare* SRNs on *C. sativus* leaves

(a) *C. sativus* cotyledons expressing HA-tagged SRNs using the *Agrobacterium*-mediated transient gene expression system. Photographs were taken at 5 dpi. Suspensions of *Agrobacteria* were infiltrated throughout the leaves. (b) Immunoblot analysis of proteins isolated from *C. sativus* cotyledons expressing SRNs. Total proteins were extracted at 5 dpi. The estimated molecular weight of each protein is as follows; SRN1-HA: 17.1 kDa, SRN2-HA: 22.9 kDa, SRN3.1-HA: 17.5 kDa, SRN3.2-HA: 14.8 kDa, SRN4-HA: 21.9 kDa. Anti-HA antibody (Roche) was used to detect tagged proteins. Coomassie-stained Rubisco large subunit (RBCL) proteins were used as loading controls. (c) Levels of *SRNs* transcripts during different infection stages of *C. orbiculare* were quantified using RT-qPCR. Total RNA was isolated from vegetative hyphae (VH) grown in vitro, conidia, and infected *C. sativus* leaves at 1, 3, and 7 dpi. To compare the number of transcripts from each gene, the copy number of each transcript was calculated using the standard curve drawn for the plasmid harboring the sequence of each transcript. Copy numbers were relative to the constitutively expressed *C. orbiculare* ribosomal protein L5 gene (Cob_v012718). Three biological replicates and two technical replicates were analyzed. Data represent mean ±SE.

420 Next, we examined the chitin-triggered ROS bursts in *C. sativus* cotyledons expressing

421 either SRN1-HA, SRN2-HA, SRN3.1-HA, SRN3.2-HA, or SRN4-HA (Fig. 4a).

422 Remarkably, *SRN1-HA* and *SRN2-HA* significantly enhanced chitin-triggered ROS

423 bursts compared to GFP controls. On the other hand, SRN3.1-HA, SRN3.2-HA, and

424 SRN4-HA did not, despite the detectable proteins accumulated (Fig. 4b). These data

425 indicated that SRN1 and SRN2 leads to immune responses in host plants.

426

427 **Enhancement of PTI by *SRN1/2* requires their catalytic residues and signal**

428 **peptides**

429 A previous report shows that two histidine residues (H40 and H92) are required for the

430 ribonuclease catalytic activity of *A. oryzae* RNase T1, a homolog of SRNs (Nishikawa

431 *et al.*, 1987). To test whether histidine-dependent ribonuclease catalytic activity is

432 involved in the ROS burst enhancement, we mutated the histidine residues of SRN1

433 corresponding to those of *A. oryzae*, H63 and H114, to alanine (SRN1$^{H63A/H114A}$).

434 Strikingly, the substitution abolished the SRN1-mediated ROS bursts (Fig. 4c). We also

435 noticed that the single mutation of H114 alone reduced the enhancement of

436 chitin-triggered ROS bursts (Fig. 4c). The similar double mutations (H92A and H130A)

437 and single mutation (H130A) in SRN2 showed the same trends (Fig. 4e). Overall, we

438 concluded that the ribonuclease catalytic residues of SRN1 and SRN2 are required for

439 the enhancement of chitin-triggered ROS bursts.

440 Next, we assessed the effect of the signal peptide of SRN1 by deleting the

441 sequence (SRN1$^{\Delta SP}$). The signal peptide-deleted SRN1 and SRN2 did not enhance

442 chitin-triggered ROS bursts (Fig. 4c). These data suggest that the enhancement of the

443 chitin-triggered response requires SRN1 and SRN2 to be external to the host cell,

444 probably in the apoplastic region. We note that none of the loss of ROS burst

445 enhancement by substitutions could be explained by the abrogation of protein

446 expression (Fig. 4d and 4f).

447 The SRN proteins expressed in our setup were predicted to be modified

448 post-translationally because all showed multiple bands larger than expected in

449 immunoblots (Fig. 3b). Given that signal peptide-dependency for the mobility shift (Fig.

450 4d), one plausible post-translational modification is glycosylation.

16

Kumakura *et al.*
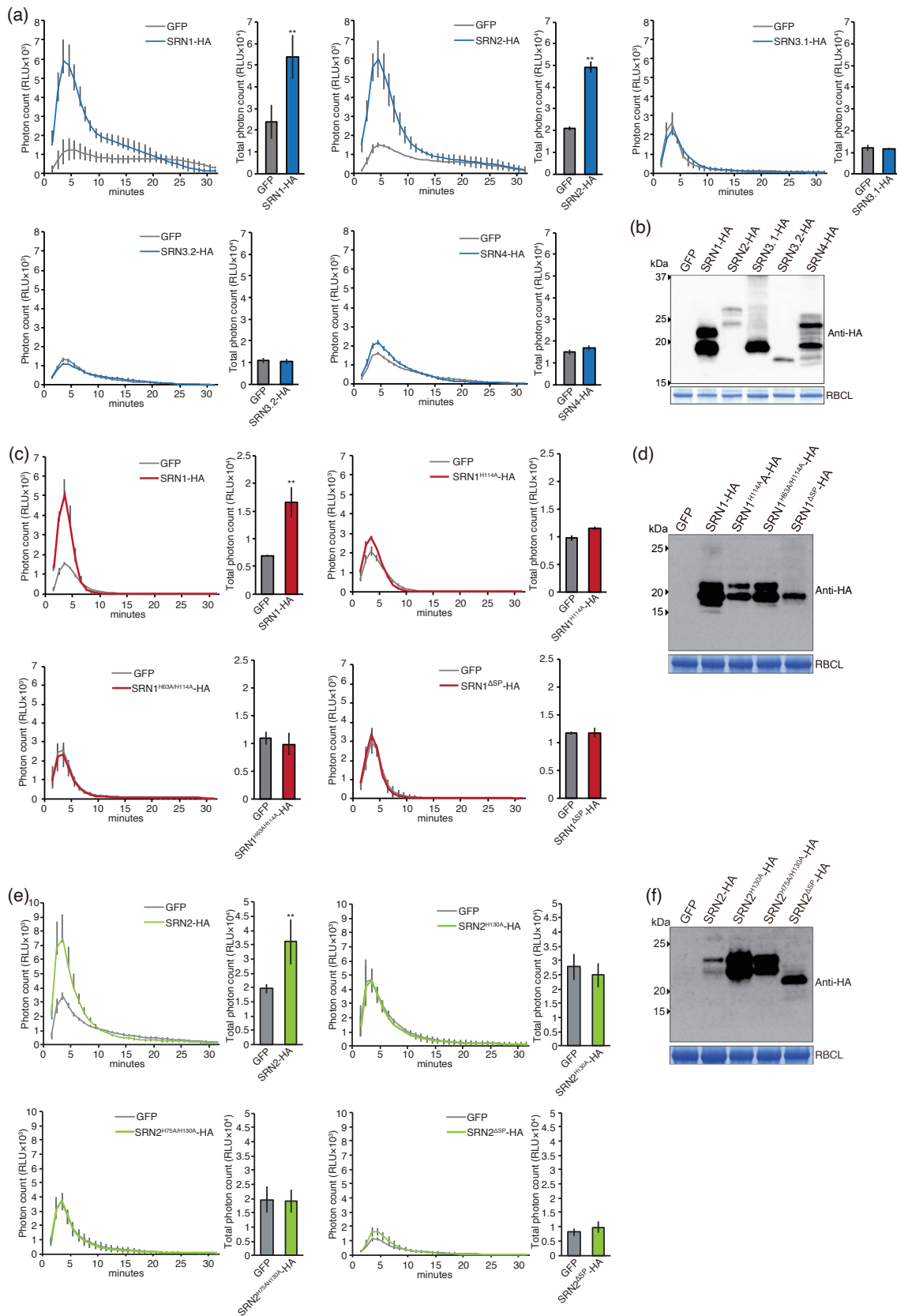
451
452 **Figure 4. SRN1 and SRN2 expression potentiates chitin-triggered ROS bursts in *C.**
453 *sativus* leaves**

17

454   (a) Enhancement of chitin-triggered ROS bursts was observed in *C. sativus* cotyledons
455   expressing SRN1-HA and SRN2-HA. Oxidative bursts were elicited by chitin (10 µM).
456   Total photon counts were the sum of RLUs (relative light units) for a 30 min
457   measurement. Three independent experiments showed similar results. Data represent
458   mean ±SE (n=3). (b) Expression of SRN1-HA, SRN2-HA, SRN3.1-HA, SRN3.2-HA,
459   and SRN4-HA proteins in *C. sativus* was confirmed by immunoblot analysis. Details of
460   the analysis are the same as for the immunoblot in Fig. 3b. (c) Ribonuclease catalytic
461   residues and the signal peptide of SRN1 are required for the chitin-triggered ROS burst
462   enhancement. The H114 ribonuclease catalytic residue of SRN1 was mutated in
463   SRN1^{H114A}-HA. Both H63 and H114 ribonuclease catalytic residues of SRN1 were
464   mutated in SRN1$^{H63A/H114A}$-HA. The predicted signal peptide of SRN1 was deleted in
465   SRN1$^{\Delta SP}$-HA. Experiments were performed as described in (a). Data represent mean
466   ±SE (n=3). (d) Protein expression from the wild-type and mutated series of SRN1
467   (SRN1-HA, SRN1^{H114A}-HA, SRN1$^{H63A/H114A}$-HA, and SRN1$^{\Delta SP}$-HA) was confirmed by
468   immunoblot analysis. The estimated molecular weight of each protein is as follows;
469   SRN1-HA, SRN1^{H114A}-HA and SRN1$^{H63A/H114A}$-HA: 17.1 kDa, SRN1$^{\Delta SP}$-HA: 15.5 kDa.
470   (e) Ribonuclease catalytic residues and the signal peptide of SRN2 were required for the
471   chitin-triggered ROS burst enhancement. The H130 ribonuclease catalytic residue of
472   SRN2 was mutated in SRN2^{H130A}-HA. Both H75 and H130 ribonuclease catalytic
473   residues of SRN2 were mutated in SRN2$^{H75A/H130A}$-HA. The predicted signal peptide of
474   SRN2 was deleted in SRN2$^{\Delta SP}$-HA. Experiments were performed as described in (a).
475   Data represent mean ±SE (n=3). (f) Expression of wild-type and mutated series of
476   SRN2 (SRN2-HA, SRN2^{H130A}-HA, SRN2$^{H75A/H130A}$-HA, and SRN2$^{\Delta SP}$-HA) was
477   confirmed by immunoblot analysis. The estimated molecular weight of each protein is
478   as follows; SRN2-HA, SRN2^{H130A}-HA, and SRN2$^{H75A/H130A}$-HA: 22.9 kDa,
479   SRN2$^{\Delta SP}$-HA: 21.2 kDa. ** indicates $p < 0.01$ (t-test) (a, c, e). Anti-HA antibody was
480   used to detect HA-tagged proteins (b, d, f). Coomassie-stained RBCL proteins were
481   used as loading controls (b, d, f).
482

483 Therefore, we predicted the glycosylation sites of SRNs using the NetNGlyc 1.0 server

484 (Gupta & Brunak, 2002) and found that SRN1, SRN3.1, SRN3.2, and SRN4 have one

485 potential glycosylated site each, while SRN2 has two. To assess whether glycosylation

486 affects the function of SRNs, we mutated the predicted glycosylation sites (N101 and

487 N143) of SRN2, as a representative of the SRNs, creating $SRN2^{N101Q/N143Q}$ (Supporting

488 Information Fig. S5a). As expected, this substitution constricted into a single protein

489 band in immunoblot (Supporting Information Fig. S5b). Moreover, the treatment by

490 deglycosylation enzyme reduced the intensity of the two bands in original SRN2 and

491 generated a lower band, which was the same size as $SRN2^{N101Q/N143Q}$ (Supporting

492 Information Fig. S5c). However, irrespective of the glycosylation, we observed the

493 immunity response by SRN2; $SRN2^{N101Q/N143Q}$ induced chitin-triggered ROS bursts at

494 the same level as the wild-type SRN2 in *C. sativus* (Supporting Information Fig. S5d-f)

495 without any visible phenotype (Supporting Information Fig. S5g). In summary, these

496 data suggest that the glycosylation of SRN2 does not affect its enhancement of

497 chitin-triggered ROS bursts when expressed in *C. sativus*.

498

499 **Chitin-triggered MPK phosphorylation and PTI marker gene expression are**

500 **enhanced by *SRN1* or *SRN2* in *C. sativus***

501 As the signaling pathways activated by PAMP perception include the activation of the

502 mitogen-activated protein kinases, MPK3, MPK4, and MPK6 in *Arabidopsis* (Asai *et*

503 *al.*, 2002; Ichimura *et al.*, 2006), we assessed the effect of SRN1 and SRN2 on

504 chitin-triggered MPK phosphorylation in *C. sativus* (Fig. 5a, b). Indeed, SRN1 and

505 SRN2 expression enhanced phosphorylation of MPKs (p44/42) upon chitin treatment,

506 whereas the catalytically dead mutants ($SRN1^{H63A/H114A}$ and $SRN2^{H75A/H130A}$) did not.

507 It is well known that downstream events after activation of the MPK signaling

508 cascade by PAMPs include transcriptional up-regulation of certain defense-related

509 genes, such as *FRK1*, *NHL10*, *CYP82*, and *PHI1* in *Arabidopsis* (Wan *et al.*, 2008).

510 Therefore, we analyzed the expression of a set of *C. sativus* homologs of these PTI

511 marker genes. We found that the expression of the *C. sativus FRK1* and *NHL10*

512 homologs, *CsFRK1* and *CsNHL10*, was strongly induced 30 min after chitin treatment

513 (Supporting Information Fig. S6). Importantly, these mRNAs were further induced by

514 wild-type SRN1 and SRN2, but not by the catalytic mutants (Fig. 5c, d).

19
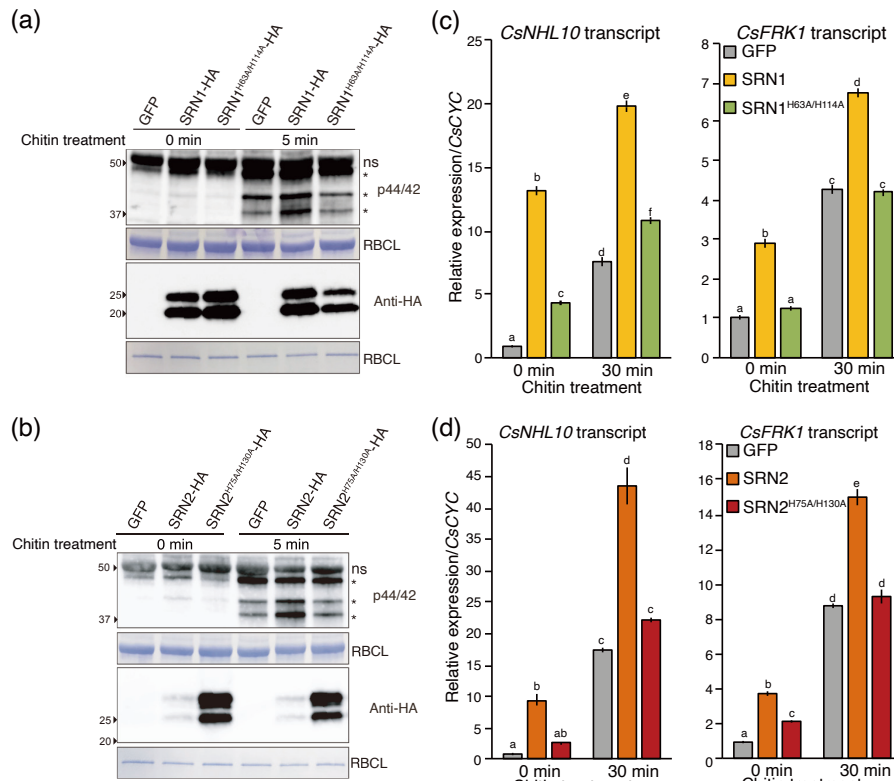
Figure 5. PTI potentiation by SRN1 and SRN2 expression in *C. sativus*

(a) Chitin-treated *C. sativus* cells expressing SRN1-HA showed enhanced MPKs phosphorylation. *C. sativus* cotyledons treated with chitin for 0 and 5 min were used. GFP, SRN1-HA, or SRN1$^{H63A/H114A}$-HA were expressed in *C. sativus* cotyledons by an *Agrobacterium*-mediated transient gene expression system. Upper panel: phosphorylation of MPKs was detected using anti-phospho-p44/42 MAPK antibody. Lower panel: anti-HA antibody was used. Coomassie-stained RBCL proteins were used as loading controls. Similar results were obtained from independent three experiments. ns indicates a non-specific band. Asterisks indicate MPKs of *C. sativus*. (b) SRN1-HA expression induced PTI marker gene accumulation in *C. sativus* cells, as for SRN1-HA in panel (a). (b, d) Accumulation of *CsNHL10* and *CsFRK1* transcripts was quantified by RT-qPCR. *CsCYC* was used as endogenous control as established in a previous report (Liang *et al.*, 2018). Primers used are listed in Supporting Information Table S3. Different lower-case letters indicate significant differences ($p < 0.05$, Tukey HSD). Data represent mean ±SE (n=3). Two independent experiments showed similar results. (c) Chitin-treated *C. sativus* cells expressing SRN2-HA showed enhanced MPKs phosphorylation. The experiment was performed as described in (a). (d) SRN2-HA expression induced PTI marker gene accumulation in *C. sativus* cells. The experiment was performed as described in (b).

537 We note that even in the absence of chitin, SRN1 and SRN2 could lead *CsNHL10* and

538 *CsFRK1* expression, suggesting the synergistic effects. Overall, these results indicates

539 that SRN1 and SRN2 potentiate PTI responses in a catalytic residue-dependent manner.

540

541 **SRN1 cleaves ssRNAs at guanosine residues and leaves 3′-phosphates at 5′**

542 **fragments**

543 To test an enzymatic activity of SRN1 in vitro, we utilized *Pichia pastoris,* which can

544 secrete the recombinant protein outside the cell by secretion signal, α-factor (Brake *et*

545 *al.*, 1984). Here we substituted intrinsic signal peptide of SRN1 with the α-factor.

546 Indeed, *P. pastoris* successfully expressed $SRN1^{\Delta SP}$ fused with α-factor at their

547 N-terminus, however, the amount did not reach enough level for further biochemical

548 use (data not shown), maybe due to cell toxicity. Therefore, a mutation, H63A, which

549 could weaken the potential ribonuclease activity and cell toxicity was introduced into

550 SRN1. H63 corresponds to H58 of *A. oryzae* RNase T1, and it has been reported that

551 the ribonuclease activity is still detected and the substrate specificity is not affected

552 when the mutation is introduced (Nishikawa *et al.*, 1987). Indeed, sufficient amounts of

553 $SRN1^{H63A/\Delta SP}$ protein were obtained for subsequent biochemical analyses. In addition to

554 the single mutant, we isolated the double mutant ($SRN1^{H63A/H114A/\Delta SP}$) as a catalytically

555 dead control.

556 Given that SRN1 homolog RNase T1 cleaves RNAs at guanosine residues

557 specifically (Nishikawa *et al.*, 1987), we reasoned that SRN1 may have the same

558 nucleotide specificity. To test this possibility, we use two different ssRNAs as

559 substrates: adenine/guanine-repeated polypurine RNA (AG10) and

560 uracil/cytosine-repeated polypyrimidine RNA (UC10), conjugated with fluorescein

561 (FAM) at their 5′ ends (Fig. 6a top). Indeed, $SRN1^{H63A/\Delta SP}$ digested AG10 but not UC10,

562 indicating its nucleotide specificity toward. In contrast, the catalytically dead

563 $SRN1^{H63A/H114A/\Delta SP}$ could not cleave the AG10 (Fig. 6a bottom). This reaction did not

564 require Mg ions, which is a key cofactor for a subset of RNases (Fig. 6a, Supporting

565 Information Fig. S7a). Titration of enzyme amount allowed us to track the reaction

566 intermediates, which corresponds to nine fragments of AG10 (Supporting Information

567 Fig. S7b), suggesting that SRN1 mediated endoribonucleolytic cleavage at adenosine or

568 guanosine residues, but not both.
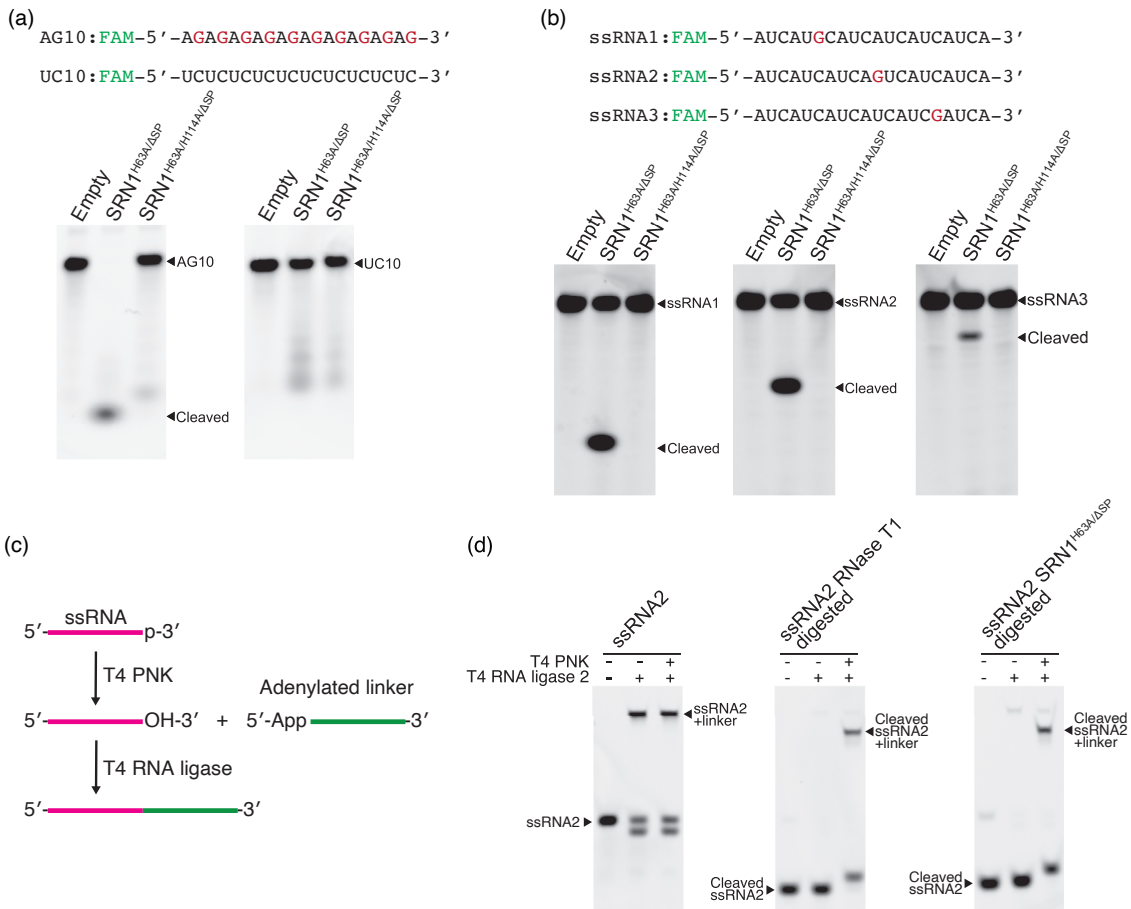
21

Figure 6. SRN1 cleaves ssRNAs at guanosine residues in vitro

(a) SRN1$^{H63A/\Delta SP}$ cleaved AG10, but did not UC10. In vitro RNase assays were performed with recombinant proteins produced by *P. pastoris* (SRN1$^{H63A/\Delta SP}$ and SRN1$^{H63A/H114A/\Delta SP}$), and chemically synthesized substrate ssRNAs (AG10 and UC10) labelled with fluorescein (FAM), at their 5′-termini. (b) SRN1$^{H63A/\Delta SP}$ cleaves ssRNAs at guanosine residues. ssRNA1, ssRNA2, and ssRNA3 have one guanosine residue, respectively, at different sites. ssRNA1, ssRNA2 and ssRNA3 are labelled with FAM at their 5′-termini. (c) Schematics of ssRNA dephosphorylation and linker ligation for (d). T4 PNK dephosphorylate 3′ end of ssRNA. T4 RNA ligase 2 conjugates the 3′-hydroxyl end of ssRNA with the pre-adenylated ssDNA linker. (d) 3′ end of cleaved ssRNA by SRN1$^{H63A/\Delta SP}$ possesses phosphate. ssRNA2 cleaved by SRN1$^{H63A/\Delta SP}$ was ligated with the pre-adenylated ssDNA only when the fragment was pre-treated with T4 PNK.

22

585   Thus, we tested whether SRN1 cleaves RNAs at guanosine residue using

586   RNA substrates that only possess single guanosine but different positions (Fig. 6b,

587   ssRNA1, ssRNA2, and ssRNA3). According to the position of the guanosine,

588   SRN1$^{H63A/\Delta SP}$ generated short, middle, and long RNA fragments from ssRNA1, ssRNA2,

589   and ssRNA3, respectively, showing that SRN1$^{H63A/\Delta SP}$ cleaves RNA at guanosine (Fig.

590   6b). We also tested whether SRN1 cleaves double stranded (ds) RNAs (Supplementary

591   Information Fig. S7c, dsRNA4). Although un-annealed single strand RNA (ssRNA4)

592   was cleaved by SRN1$^{H63A/\Delta SP}$ as expected, dsRNA4 was tolerate (Supplementary

593   Information Fig. S7c). Thus, we concluded that SRN1 is a single-stranded

594   RNA-specific endoribonuclease that cleaves at guanosine.

595   Considering that endonucleolytic cleavage by RNase T1 results in 3′-end

596   phosphate at the 5′ RNA fragment (Nishikawa *et al.*, 1987), we further investigated the

597   molecular form of the cleaved end by SRN1. For this purpose, we harnessed the

598   ligation-based assay; 3′ phosphate hampers the ligation to 3′ DNA fragment by T4 RNA

599   ligase 2, whereas 3′ hydroxy group is susceptible to the reaction (Fig. 6c). As expected,

600   the RNA (ssRNA2) that has a 3′-hydroxyl end was ligated (Fig. 6d, left panel). In

601   contrast, the RNase T1-cleaved RNA could not engage in this ligation reaction unless

602   the 3′ end is dephosphorylated by T4 polynucleotide kinase (PNK) (Fig. 6d, middle

603   panel). Similarly, SRN1$^{H63A/\Delta SP}$ generated RNAs in the 3′-end form that could be ligated

604   only after T4 PNK treatment (Fig. 6d, right panel). The striking correspondence of the

605   substrate specificity (single stranded guanosine) (Fig. 6b), metal ion independency (Fig.

606   6a and Supporting Information Fig. S7a), and 3′-end phosphate in the cleaved product

607   (Fig. 6d) showed that SRN1 functionally resembles RNase T1 (Nishikawa *et al.*, 1987).

608

609   **The *srn1 srn2* double mutant strains show increased invasion and relative fungal**

610   **biomass *in planta***

611   To assess the biological relevance of our findings, we established *srn1*, *srn2*, and *srn1*

612   *srn2* double knockout mutants and performed infection assays. We measured the

613   invasion ratio, the percentage of successful infection hyphae per appressorium (Fig. 7a),

614   at the early infection stage when the expression of *SRN1* and *SRN2* is induced (Fig. 3c).

615   The invasion ratios were significantly increased in the two independent *srn1 srn2*

616   double mutant strains (Fig. 7b).
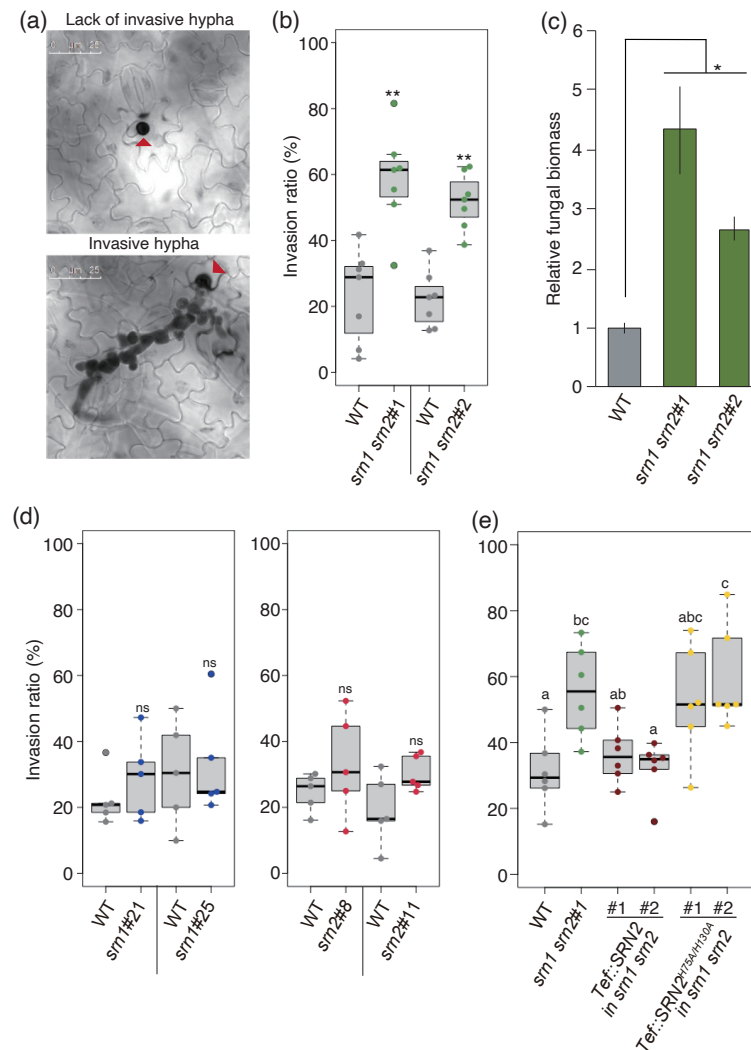
Figure 7. *C. orbiculare srn1 srn2* mutants showed increased virulence

(a) Example of lack of invasive hypha (top) and invasive hypha (bottom) formation from *C. orbiculare* appressoria. Red arrowheads indicate appressoria. Invasive hypha from successfully invaded appressoria were observed in the bottom panel. *C. sativus* cotyledons inoculated with *C. orbiculare* were trypan blue stained in both panels. Scale bars represent 25 μm. (b and d) Invasion ratio of a series of *srn* mutants on *C. sativus* cotyledons at 60 hpi. Leaves were inoculated with 5 μl of conidial suspensions at 1×10^5 conidia ml^{-1}. Each boxplot includes six to eight replicates. Each replicate was calculated using at least 50 appressoria. The box contains data within 1st and 3rd quartiles. *, **, and ns indicate $p < 0.05$, $p < 0.01$, and not significant compared to *C. orbiculare* WT, respectively (t-test). (c) Fungal biomass during infection was quantified by RT-qPCR. A section of the ribosomal protein L5 transcript of *C. orbiculare* and a section of the *CsCYC* transcript of *C. sativus* were used for quantification. Primers used are listed in Supporting Information Table S4. Total RNAs were extracted from

632 cotyledons inoculated either with *C. orbiculare* wild type or two *srn1 srn2* mutant
633 strains at 88 hpi. * indicates p < 0.05 (t-test) compared to *C. orbiculare* WT. Data
634 represent mean ±SE (n=6). (e) Overexpression of *SRN2* in *srn1 srn2* reduced the
635 increased invasion ratio of the *srn1 srn2* mutant. *Tef* promoter-driven *SRN2* or
636 *SRN2^{H75A/H130A}* were expressed in the *srn1 srn2*#1 mutant. The invasion ratio was
637 measured using the same method as described in (b, d). Different lower-case letters
638 indicate significant differences (p < 0.05, Tukey HSD).

640 In contrast, the *srn1* and *srn2* single mutants did not significantly alter the invasion
641 ratios (Fig. 7d), suggesting the redundant functions of *SRN1* and *SRN2*.

642   To further ensure the role of *SRNs* in infection, we overexpressed *SRN2* in
643 *srn1 srn2* double knockout strain. Here, ectopic *SRN2* was expressed by the promoter of
644 *Aureobasidium pullulans TRANSLATION ELONGATION FACTOR* (*Tef*)
645 (Wymelenberg *et al.*, 1997). Indeed, the overexpression of SRN2 in the double
646 knockout cells (denoted as *Tef::SRN2* in *srn1 srn2*#1 and #2) showed decreased
647 invasion ratios compared to the parental double knockout mutant (*srn1 srn2*#1) (Fig.
648 7e). In contrast, catalytic inactive SRN2 (*Tef::SRN2^{H75A/H130A}* in *srn1 srn2*) could not
649 complement the phenotype (Fig. 7e), suggesting the ribonuclease catalytic residues or
650 activity are monitored by host to drive the immunity.

651   We also assessed the relative fungal biomass levels, which was probed by *C.*
652 *orbiculare* transcripts (especially ribosome protein L5), during infection on *C. sativus*
653 leaves. Consistent with the invasion ratios, *srn1 srn2* double mutants showed
654 significantly increased fungal biomass (Fig. 7c). Collectively, our data indicates that
655 *SRN1* and *SRN2* in *C. sativus* enhance defense responses of the host plant to this fungi.

657 **Discussion**
658 Plants often perceive the presence of pathogens by recognizing molecules or the
659 enzymatic activities of proteins originating from pathogens. Here, we report that *C.*
660 *orbiculare* ribonuclease effectors, SRN1 and SRN2, potentiate typical PTI responses of
661 *C. sativus* in a manner that is dependent on their catalytic residues and signal peptides.
662 Our genetic analysis revealed that the *srn1 srn2* double mutants showed increased
663 invasion ratios and relative fungal biomass (Fig. 7b, c), suggesting that SRN1 and
664 SRN2 can be detrimental to the pathogen. Consistent with this notion, expression of

665   SRN1 and SRN2 in *C. sativus* enhanced chitin-triggered ROS bursts (Fig. 4a) and MPK

666   phosphorylation (Fig. 5a, b), as well as PTI marker gene expression (Fig. 5c, d). As

667   these effects require catalytic residues and the signal peptides of SRN1 and SRN2, their

668   enzymatic activity is likely to be recognized in the outside of the host cells (Fig. 4c, e),

669   most probably in its apoplastic region. In line with this, in vitro analysis revealed that

670   SRN1 recombinant proteins have an endoribonuclease activity that specifically cleaves

671   ssRNAs at guanosine producing oligonucleotides with 3′ phosphate.

672   The action of SRN1 and SRN2 is apparently different from that of three

673   ribonuclease-type effectors reported previously. Firstly, Zt6 from *Zymoseptoria tritici* is

674   reported to be a host cell death-inducing effector by degrading rRNA in the host cells

675   (Kettles *et al.*, 2018). In contrast, SRN1 and SNR2 did not induce cell death in their

676   host, *C. sativus*. In the *N. benthamiana* expression system, SRN2 induced cell death but

677   their full cell death activity required signal peptide (Supporting Information Fig. S8),

678   indicating that the effector targets are likely to be apoplastic RNAs, rather than cellular

679   (r)RNA in the host. Secondly, CSEP0064/BEC1054, one of the 27 *Blumeria graminis*

680   ribonuclease-like effectors that lack catalytic active residues, acts as a virulence factor

681   inside the host cells (Pedersen *et al.*, 2012; Pliego *et al.*, 2013). More recently,

682   Pennington *et al.* (2019) showed that CSEP0064/BEC1054 binds nucleic acids and

683   inhibits   the   degradation   of   host   rRNA   induced   by   plant   endogenous

684   ribosome-inactivating proteins (RIPs) (Pennington *et al.*, 2019). Based on these findings,

685   Pennington *et al.* (2019) proposed that CSEP0064/BEC1054 is a pseudoenzyme that

686   interacts with host ribosomes and inhibits the action of RIPs. Thirdly, AvrPm2, another

687   ribonuclease-like protein of *B. graminis*, is recognized by the barley nucleotide-binding,

688   leucine-rich repeat receptor (NLR) protein, Pm2 in the host cell (Praz *et al.*, 2016),

689   suggesting that AvrPm2 is a cytoplasmic effector that causes hypersensitive cell death

690   triggered by an NLR. Thus, these three effectors are all predicted to be cytoplasmic

691   effectors and are thus different from SRNs.

692   Host-specific cell death (only found in *N. benthamiana* but not in *C. sativus*) by

693   SRNs expression remains an open question. One plausible explanation is that *N.*

694   *benthamiana* encodes an as yet unidentified PRR that is able to trigger cell death upon

695   direct or indirect detection of SRNs. Such cell death-inducing PRRs have been known

696   in several species including potato and rice (Song *et al.*, 1995; Du *et al.*, 2015). In this

697 scenario, it is also possible that *C. sativus* may encode a similar PRR that can detect the

698 activity of *SRN1* and *SRN2* in the apoplast but potentiate PTI without causing cell death.

699 As both signal peptides and catalytic residues of SRN1 and SRN2 are required for the

700 full cell death activity in *N. benthamiana* and for PTI potentiation in *C. sativus*, it is

701 possible that SRN1 and SRN2 cleaves RNAs in the apoplast and the resulting RNA

702 molecules trigger immune responses via a PRR. In *Arabidopsis*, virus-derived dsRNAs

703 induce PTI responses via SERK1, a receptor like kinase (Niehl *et al.*, 2016). In addition,

704 bacterial RNAs also induce immune responses in *Arabidopsis* when infiltrated into

705 leaves (Lee *et al.*, 2016). Thus, plants may be able to perceive certain RNA molecules

706 in the apoplast. If RNAs are derived from host plants, these molecules may serve as

707 DAMPs to indirectly detect invasive pathogens secreting specific RNases in the

708 apoplast. This is a plausible case for SRNs, which are guanosine-specific single-strand

709 endoribonucleases leaving 3′ phosphate, as plants normally do not encode RNases with

710 this specificity. In mammals, PRRs such as Toll-like receptor (TLR) 3 and TLR7 can

711 detect virus-derived dsRNA and ssRNAs, respectively (Takeuchi & Akira, 2010;

712 Alexopoulou *et al.*, 2001; Diebold & Brencicova, 2013). Isolation of such plant PRRs in

713 the future will help to clarify the similarities and differences between the ways plants

714 and animals recognize RNA molecules.

715   Why did all the *Colletotrichum* species we investigated encode SRN proteins?

716 Although we did not detect a virulence function of SRN1 and SRN2 in our pathosystem,

717 these proteins should provide biological advantage to the pathogen. For example, the

718 function of these proteins is possibly manipulation of the local microbial community, as

719 shown for Zt6 (Kettles *et al.*, 2018; Snelders *et al.*, 2018). Alternatively, SRNs target

720 their own secreted RNAs. Fungal pathogens, such as *Botrytis cinerea*, can secrete small

721 RNAs as effectors suppressing host immune responses (Weiberg *et al.*, 2013). Thus,

722 SRNs could be used to process such RNAs, which may serve as PAMPs when the host

723 contains corresponding PRRs. However, if this is the case, it is difficult to explain why

724 transient expression of SRNs in the host in the absence of a pathogen can induce

725 immune responses. In addition, if SRNs are involved in the production of pathogen

726 RNA effectors, the knockout phenotype is predicted to reduce virulence. However, the

727 phenotype we observed was gain of virulence (Fig. 7). Another possibility is that SRNs

728 target host apoplastic RNAs. *A. thaliana* apoplastic fluid contains both sRNAs and

27

729 lncRNAs associated with proteins (Karimi *et al.*, 2021). sRNAs of host plants were also

730 detected in *Verticillium dahliae* and could down-regulate virulence-related genes

731 (Zhang *et al.*, 2016). Thus, such host-derived defensive apoplastic RNAs can be

732 potential targets of SRNs. In this scenario, degrading host RNAs should increase

733 pathogen virulence *per se*. Such virulence effects of SRNs may be observed in a host

734 that is not able to detect the ribonuclease activity of SRNs. The identification of the

735 target RNAs of SRNs will further clarify RNA-mediated plant-microbe interactions.

736

737 **Acknowledgements**

752

753 **Author Contributions**

754 NK, SO, YT, and KS designed the research. NK, SO, and MN performed experiments.

755 PG and AT analyzed genome and transcriptome data. NK, NI, SW and MS prepared

756 recombinant proteins. NK and SI performed in vitro analysis. YN, YT, and KS

757 supervised the project. NK, PG, and KS wrote the manuscript with the edition from all

758 the authors.

759

760 **Data Availability Statement**

761   The data that supports the findings of this study are available in the supplementary

762   material of this article or from the corresponding author upon reasonable request.

763

764   **References**

765   **Alexopoulou L, Holt AC, Medzhitov R, Flavell RA**. **2001**. Recognition of
766   double-stranded RNA and activation of NF-κB by Toll-like receptor 3. *Nature* **413**:
767   732–738.

768   **Amselem J, Cuomo CA, Kan JAL van, Viaud M, Benito EP, Couloux A, Coutinho
769   PM, Vries RP de, Dyer PS, Fillinger S, *et al.* 2011**. Genomic analysis of the
770   necrotrophic fungal pathogens *Sclerotinia sclerotiorum* and *Botrytis cinerea*. *PLOS
771   Genetics* **7**: e1002230.

772   **Arnaud MB, Cerqueira GC, Inglis DO, Skrzypek MS, Binkley J, Chibucos MC,
773   Crabtree J, Howarth C, Orvis J, Shah P, *et al.* 2012**. The *Aspergillus* Genome
774   Database (AspGD): recent developments in comprehensive multispecies curation,
775   comparative genomics and community resources. *Nucleic Acids Research* **40**:
776   D653–D659.

777   **Asai T, Tena G, Plotnikova J, Willmann MR, Chiu W-L, Gomez-Gomez L, Boller
778   T, Ausubel FM, Sheen J**. **2002**. MAP kinase signalling cascade in *Arabidopsis* innate
779   immunity. *Nature* **415**: 977–983.

780   **Baldrich P, Rutter BD, Karimi HZ, Podicheti R, Meyers BC, Innes RW**. **2019**.
781   Plant extracellular vesicles contain diverse small RNA species and are enriched in 10-
782   to 17-nucleotide "tiny" RNAs. *The Plant Cell* **31**: 315–324.

783   **Baroncelli R, Amby DB, Zapparata A, Sarrocco S, Vannacci G, Le Floch G,
784   Harrison RJ, Holub E, Sukno SA, Sreenivasaprasad S, *et al.* 2016**. Gene family
785   expansions and contractions are associated with host range in plant pathogens of the
786   genus *Colletotrichum*. *BMC Genomics* **17**: 555.

787   **Baroncelli R, Sreenivasaprasad S, Sukno SA, Thon MR, Holub E**. **2014**. Draft
788   genome sequence of *Colletotrichum acutatum sensu lato* (*Colletotrichum fioriniae*).
789   *Genome Announcements* **2**: e00112-14.

790   **Beimforde C, Feldberg K, Nylinder S, Rikkinen J, Tuovila H, Dörfelt H, Gube M,
791   Jackson DJ, Reitner J, Seyfullah LJ, *et al.* 2014**. Estimating the Phanerozoic history
792   of the Ascomycota lineages: Combining fossil and molecular data. *Molecular
793   Phylogenetics and Evolution* **78**: 386–398.

794   **Berka RM, Grigoriev IV, Otillar R, Salamov A, Grimwood J, Reid I, Ishmael N,
795   John T, Darmond C, Moisan M-C, *et al.* 2011**. Comparative genomic analysis of the
796   thermophilic biomass-degrading fungi *Myceliophthora thermophila* and *Thielavia
797   terrestris*. *Nature Biotechnology* **29**: 922–927.

798   **Blanco-Ulate B, Rolshausen PE, Cantu D**. **2013**. Draft genome sequence of the
799   grapevine dieback fungus *Eutypa lata* UCR-EL1. *Genome Announcements* **1**:
800   e00228-13.

801   **Boutrot F, Zipfel C**. **2017**. Function, discovery, and exploitation of plant pattern
802   recognition receptors for broad-spectrum disease resistance. *Annual Review of
803   Phytopathology* **55**: 257–286.

Brake AJ, Merryweather JP, Coit DG, Heberlein UA, Masiarz FR, Mullenbach GT, Urdea MS, Valenzuela P, Barr PJ. **1984**. Alpha-factor-directed synthesis and secretion of mature foreign proteins in *Saccharomyces cerevisiae*. *Proceedings of the National Academy of Sciences, USA* **81**: 4642–4646.

Cai Q, Qiao L, Wang M, He B, Lin F-M, Palmquist J, Huang H-D, Jin H. **2018**. Plants send small RNAs in extracellular vesicles to fungal pathogen to silence virulence genes. *Science*: eaar4142.

Cannon PF, Damm U, Johnston PR, Weir BS. **2012**. *Colletotrichum* – current status and future directions. *Studies in Mycology* **73**: 181–213.

Capella-Gutiérrez S, Silla-Martínez JM, Gabaldón T. **2009**. trimAl: a tool for automated alignment trimming in large-scale phylogenetic analyses. *Bioinformatics* **25**: 1972–1973.

Chen J, Inoue Y, Kumakura N, Mise K, Shirasu K, Takano Y. **2021**. Comparative transient expression analyses on two conserved effectors of *Colletotrichum orbiculare* reveal their distinct cell death-inducing activities between *Nicotiana benthamiana* and melon. *Molecular Plant Pathology* **in press**.

Cissé OH, Almeida JMGCF, Fonseca Á, Kumar AA, Salojärvi J, Overmyer K, Hauser PM, Pagni M. **2013**. Genome sequencing of the plant pathogen *Taphrina deformans*, the causal agent of peach leaf curl. *mBio* **4**: e00055-13.

Coleman JJ, Rounsley SD, Rodriguez-Carres M, Kuo A, Wasmann CC, Grimwood J, Schmutz J, Taga M, White GJ, Zhou S, *et al.* 2009. The genome of *Nectria haematococca*: contribution of supernumerary chromosomes to gene expansion. *PLOS Genetics* **5**: e1000618.

Cuomo CA, Güldener U, Xu J-R, Trail F, Turgeon BG, Pietro AD, Walton JD, Ma L-J, Baker SE, Rep M, *et al.* 2007. The *Fusarium graminearum* genome reveals a link between localized polymorphism and pathogen specialization. *Science* **317**: 1400–1402.

Dean R, Kan V, L JA, Pretorius ZA, Hammond-Kosack KE, Di Pietro A, Spanu PD, Rudd JJ, Dickman M, Kahmann R, *et al.* 2012. The Top 10 fungal pathogens in molecular plant pathology. *Molecular Plant Pathology* **13**: 414–430.

Dean RA, Talbot NJ, Ebbole DJ, Farman ML, Mitchell TK, Orbach MJ, Thon M, Kulkarni R, Xu J-R, Pan H, *et al.* 2005. The genome sequence of the rice blast fungus *Magnaporthe grisea*. *Nature* **434**: 980–986.

Diebold SS, Brencicova E. **2013**. Nucleic acids and endosomal pattern recognition: how to tell friend from foe? *Frontiers in Cellular and Infection Microbiology* **3**.

Dixon MS, Golstein C, Thomas CM, Biezen EA van der, Jones JDG. **2000**. Genetic complexity of pathogen perception by plants: The example of Rcr3, a tomato gene required specifically by Cf-2. *Proceedings of the National Academy of Sciences, USA* **97**: 8807–8814.

Du J, Verzaux E, Chaparro-Garcia A, Bijsterbosch G, Keizer LCP, Zhou J, Liebrand TWH, Xie C, Govers F, Robatzek S, *et al.* 2015. Elicitin recognition confers enhanced resistance to *Phytophthora infestans* in potato. *Nature Plants* **1**: 15034.

Duplessis S, Cuomo CA, Lin Y-C, Aerts A, Tisserant E, Veneault-Fourrey C, Joly DL, Hacquard S, Amselem J, Cantarel BL, *et al.* 2011. Obligate biotrophy features

848 unraveled by the genomic analysis of rust fungi. *Proceedings of the National Academy*
849 *of Sciences, USA* **108**: 9166–9171.

850 **Eddy SR**. **2011**. Accelerated profile HMM searches. *PLOS Computational Biology* **7**:
851 e1002195.

852 **Espagne E, Lespinet O, Malagnac F, Da Silva C, Jaillon O, Porcel BM, Couloux A,**
853 **Aury J-M, Ségurens B, Poulain J, *et al.* 2008**. The genome sequence of the model
854 ascomycete fungus *Podospora anserina*. *Genome Biology* **9**: R77.

855 **Finn RD, Bateman A, Clements J, Coggill P, Eberhardt RY, Eddy SR, Heger A,**
856 **Hetherington K, Holm L, Mistry J, *et al.* 2014**. Pfam: the protein families database.
857 *Nucleic Acids Research* **42**: D222–D230.

858 **Galagan JE, Calvo SE, Borkovich KA, Selker EU, Read ND, Jaffe D, FitzHugh W,**
859 **Ma L-J, Smirnov S, Purcell S, *et al.* 2003**. The genome sequence of the filamentous
860 fungus *Neurospora crassa*. *Nature* **422**: 859.

861 **Gan P, Hiroyama R, Tsushima A, Masuda S, Shibata A, Ueno A, Kumakura N,**
862 **Narusaka M, Hoat TX, Narusaka Y, *et al.* 2021**. Telomeres and a repeat-rich
863 chromosome encode effector gene clusters in plant pathogenic *Colletotrichum* fungi.
864 *Environmental Microbiology* doi: 10.1111/1462-2920.15490.

865 **Gan P, Ikeda K, Irieda H, Narusaka M, O'Connell RJ, Narusaka Y, Takano Y,**
866 **Kubo Y, Shirasu K**. **2013**. Comparative genomic and transcriptomic analyses reveal
867 the hemibiotrophic stage shift of *Colletotrichum* fungi. *New Phytologist* **197**:
868 1236–1249.

869 **Gan P, Narusaka M, Kumakura N, Tsushima A, Takano Y, Narusaka Y, Shirasu**
870 **K**. **2016**. Genus-wide comparative genome analyses of *Colletotrichum* species reveal
871 specific gene family losses and gains during adaptation to specific infection lifestyles.
872 *Genome Biology and Evolution* **8**: 1467–1481.

873 **Gan P, Narusaka M, Tsushima A, Narusaka Y, Takano Y, Shirasu K**. **2017**. Draft
874 genome assembly of *Colletotrichum chlorophyti*, a pathogen of herbaceous plants.
875 *Genome Announcements* **5**: e01733-16.

876 **Gazis R, Kuo A, Riley R, LaButti K, Lipzen A, Lin J, Amirebrahimi M, Hesse CN,**
877 **Spatafora JW, Henrissat B, *et al.* 2016**. The genome of *Xylona heveae* provides a
878 window into fungal endophytism. *Fungal Biology* **120**: 26–42.

879 **Goffeau A, Barrell BG, Bussey H, Davis RW, Dujon B, Feldmann H, Galibert F,**
880 **Hoheisel JD, Jacq C, Johnston M, *et al.* 1996**. Life with 6000 genes. *Science* **274**:
881 546–567.

882 **Goodwin SB, M'Barek SB, Dhillon B, Wittenberg AHJ, Crane CF, Hane JK,**
883 **Foster AJ, Lee TAJV der, Grimwood J, Aerts A, *et al.* 2011**. Finished genome of the
884 fungal wheat pathogen *Mycosphaerella graminicola* reveals dispensome structure,
885 chromosome plasticity, and stealth pathogenesis. *PLOS Genetics* **7**: e1002070.

886 **Gupta R, Brunak S**. **2002**. Prediction of glycosylation across the human proteome and
887 the correlation to protein function. *Pacific Symposium on Biocomputing. Pacific*
888 *Symposium on Biocomputing*: 310–322.

889 **Hacquard S, Kracher B, Hiruma K, Münch PC, Garrido-Oter R, Thon MR,**
890 **Weimann A, Damm U, Dallery J-F, Hainaut M, *et al.* 2016**. Survival trade-offs in

891 plant roots during colonization by closely related beneficial and pathogenic fungi.
892 *Nature Communications* **7**: 11362.

893 **Hu X, Xiao G, Zheng P, Shang Y, Su Y, Zhang X, Liu X, Zhan S, St. Leger RJ,**
894 **Wang C**. **2014**. Trajectory and genomic determinants of fungal-pathogen speciation and
895 host adaptation. *Proceedings of the National Academy of Sciences, USA* **111**:
896 16796–16801.

897 **Ichimura K, Casais C, Peck SC, Shinozaki K, Shirasu K**. **2006**. MEKK1 is required
898 for MPK4 activation and regulates tissue-specific and temperature-dependent cell death
899 in *Arabidopsis*. *Journal of Biological Chemistry* **281**: 36969–36976.

900 **Irieda H, Inoue Y, Mori M, Yamada K, Oshikawa Y, Saitoh H, Uemura A,**
901 **Terauchi R, Kitakura S, Kosaka A, *et al.* 2019**. Conserved fungal effector suppresses
902 PAMP-triggered immunity by targeting plant immune kinases. *Proceedings of the*
903 *National Academy of Sciences, USA* **116**: 496–505.

904 **Kadota Y, Liebrand TWH, Goto Y, Sklenar J, Derbyshire P, Menke FLH, Torres**
905 **M-A, Molina A, Zipfel C, Coaker G, *et al.* 2018**. Quantitative phosphoproteomic
906 analysis reveals common regulatory mechanisms between effector- and
907 PAMP-triggered immunity in plants. *New Phytologist* **221**: 2160–2175.

908 **Kämper J, Kahmann R, Bölker M, Ma L-J, Brefort T, Saville BJ, Banuett F,**
909 **Kronstad JW, Gold SE, Müller O, *et al.* 2006**. Insights from the genome of the
910 biotrophic fungal plant pathogen *Ustilago maydis*. *Nature* **444**: 97–101.

911 **Karimi HZ, Baldrich P, Rutter BD, Borniego L, Zajt KK, Meyers BC, Innes RW**.
912 **2021**. Arabidopsis apoplastic fluid contains sRNA- and circular RNA-protein
913 complexes that are located outside extracellular vesicles. *bioRxiv* doi:
914 10.1101/2021.10.02.462881.

915 **Katoh K, Misawa K, Kuma K, Miyata T**. **2002**. MAFFT: a novel method for rapid
916 multiple sequence alignment on fast Fourier transform. *Nucleic Acids Research* **30**:
917 3059–3066.

918 **Kettles GJ, Bayon C, Sparks CA, Canning G, Kanyuka K, Rudd JJ**. **2018**.
919 Characterization of an antimicrobial and phytotoxic ribonuclease secreted by the fungal
920 wheat pathogen *Zymoseptoria tritici*. *New Phytologist* **217**: 320–331.

921 **Kleemann J, Rincon-Rivera LJ, Takahara H, Neumann U, Themaat EVL van,**
922 **Does HC van der, Hacquard S, Stüber K, Will I, Schmalenbach W, *et al.* 2012**.
923 Sequential delivery of host-induced virulence effectors by appressoria and intracellular
924 hyphae of the phytopathogen *Colletotrichum higginsianum*. *PLOS Pathogens* **8**:
925 e1002643.

926 **Klosterman SJ, Subbarao KV, Kang S, Veronese P, Gold SE, Thomma BPHJ,**
927 **Chen Z, Henrissat B, Lee Y-H, Park J, *et al.* 2011**. Comparative genomics yields
928 insights into niche adaptation of plant vascular wilt pathogens. *PLOS Pathogens* **7**:
929 e1002137.

930 **Kubicek CP, Herrera-Estrella A, Seidl-Seiboth V, Martinez DA, Druzhinina IS,**
931 **Thon M, Zeilinger S, Casas-Flores S, Horwitz BA, Mukherjee PK, *et al.* 2011**.
932 Comparative genome sequence analysis underscores mycoparasitism as the ancestral
933 life style of *Trichoderma*. *Genome Biology* **12**: R40.

934 **Kumakura N, Ueno A, Shirasu K**. **2019**. Establishment of a selection marker
935 recycling system for sequential transformation of the plant-pathogenic fungus
936 *Colletotrichum orbiculare*. *Molecular Plant Pathology* **20**: 447–459.

937 **Kumar S, Stecher G, Tamura K**. **2016**. MEGA7: Molecular evolutionary genetics
938 analysis version 7.0 for bigger datasets. *Molecular Biology and Evolution* **33**:
939 1870–1874.

940 **Lee B, Park Y-S, Lee S, Song GC, Ryu C-M**. **2016**. Bacterial RNAs activate innate
941 immunity in Arabidopsis. *New Phytologist* **209**: 785–797.

942 **Letunic I, Bork P**. **2016**. Interactive tree of life (iTOL) v3: an online tool for the
943 display and annotation of phylogenetic and other trees. *Nucleic Acids Research* **44**:
944 W242–W245.

945 **Li L, Stoeckert CJ, Roos DS**. **2003**. OrthoMCL: identification of ortholog groups for
946 eukaryotic genomes. *Genome research* **13**: 2178–2189.

947 **Liang C, Hao J, Meng Y, Luo L, Li J**. **2018**. Identifying optimal reference genes for
948 the normalization of microRNA expression in cucumber under viral stress. *PLOS ONE*
949 **13**: e0194436.

950 **Loftus BJ, Fung E, Roncaglia P, Rowley D, Amedeo P, Bruno D, Vamathevan J,**
951 **Miranda M, Anderson IJ, Fraser JA, *et al.* 2005**. The genome of the
952 Basidiomycetous yeast and Human Pathogen *Cryptococcus neoformans*. *Science* **307**:
953 1321–1324.

954 **Marchler-Bauer A, Bo Y, Han L, He J, Lanczycki CJ, Lu S, Chitsaz F, Derbyshire**
955 **MK, Geer RC, Gonzales NR, *et al.* 2017**. CDD/SPARCLE: functional classification of
956 proteins via subfamily domain architectures. *Nucleic Acids Research* **45**: D200–D203.

957 **Martin F, Kohler A, Murat C, Balestrini R, Coutinho PM, Jaillon O, Montanini B,**
958 **Morin E, Noel B, Percudani R, *et al.* 2010**. Périgord black truffle genome uncovers
959 evolutionary origins and mechanisms of symbiosis. *Nature* **464**: 1033–1038.

960 **Mistry J, Chuguransky S, Williams L, Qureshi M, Salazar GA, Sonnhammer ELL,**
961 **Tosatto SCE, Paladin L, Raj S, Richardson LJ, *et al.* 2021**. Pfam: The protein
962 families database in 2021. *Nucleic Acids Research* **49**: D412–D419.

963 **Mito M, Mishima Y, Iwasaki S**. **2020**. Protocol for disome profiling to survey
964 ribosome collision in humans and zebrafish. *STAR Protocols* **1**: 100168.

965 **Niehl A, Wyrsch I, Boller T, Heinlein M**. **2016**. Double-stranded RNAs induce a
966 pattern-triggered immune signaling pathway in plants. *New Phytologist* **211**:
967 1008–1019.

968 **Nishikawa S, Morioka H, Kim HJ, Fuchimura K, Tanaka T, Uesugi S, Hakoshima**
969 **T, Tomita K, Ohtsuka E, Ikehara M**. **1987**. Two histidine residues are essential for
970 ribonuclease T1 activity as is the case for ribonuclease A. *Biochemistry* **26**: 8620–8624.

971 **Noguchi S, Satow Y, Uchida T, Sasaki C, Matsuzaki T**. **1995**. Crystal structure of
972 *Ustilago sphaerogena ribonuclease* U2 at 1.8 A resolution. *Biochemistry* **34**:
973 15583–15591.

974 **Nonaka S, Someya T, Zhou S, Takayama M, Nakamura K, Ezura H**. **2017**. An
975 *Agrobacterium tumefaciens* strain with gamma-aminobutyric acid transaminase activity
976 shows an enhanced genetic transformation ability in plants. *Scientific Reports* **7**.

977 **O'Connell RJ, Thon MR, Hacquard S, Amyotte SG, Kleemann J, Torres MF,**
978 **Damm U, Buiate EA, Epstein L, Alkan N, *et al.* 2012**. Lifestyle transitions in plant
979 pathogenic *Colletotrichum* fungi deciphered by genome and transcriptome analyses.
980 *Nature Genetics* **44**: 1060–1065.

981 **Pedersen C, van Themaat EVL, McGuffin LJ, Abbott JC, Burgis TA, Barton G,**
982 **Bindschedler LV, Lu X, Maekawa T, Weßling R, *et al.* 2012**. Structure and evolution
983 of barley powdery mildew effector candidates. *BMC Genomics* **13**: 694.

984 **Pennington HG, Jones R, Kwon S, Bonciani G, Thieron H, Chandler T, Luong P,**
985 **Morgan SN, Przydacz M, Bozkurt T, *et al.* 2019**. The fungal ribonuclease-like
986 effector protein CSEP0064/BEC1054 represses plant immunity and interferes with
987 degradation of host ribosomal RNA. *PLOS Pathogens* **15**: e1007620.

988 **Petersen TN, Brunak S, von Heijne G, Nielsen H**. **2011**. SignalP 4.0: discriminating
989 signal peptides from transmembrane regions. *Nature Methods* **8**: 785–786.

990 **Pliego C, Nowara D, Bonciani G, Gheorghe DM, Xu R, Surana P, Whigham E,**
991 **Nettleton D, Bogdanove AJ, Wise RP, *et al.* 2013**. Host-induced gene silencing in
992 barley powdery mildew reveals a class of ribonuclease-like effectors. *Molecular*
993 *Plant-Microbe Interactions* **26**: 633–642.

994 **Praz CR, Bourras S, Zeng F, Sánchez-Martín J, Menardo F, Xue M, Yang L,**
995 **Roffler S, Böni R, Herren G, *et al.* 2016**. *AvrPm2* encodes an RNase-like avirulence
996 effector which is conserved in the two different specialized forms of wheat and rye
997 powdery mildew fungus. *New Phytologist* **213**: 1301–1314.

998 **Rambaut, Andrew**. FigTree. *Molecular evolution, phylogenetics and epidemiology*.

999 **Rooney HCE, Klooster JW van't, Hoorn RAL van der, Joosten MHAJ, Jones JDG,**
1000 **Wit PJGM de**. **2005**. Cladosporium Avr2 inhibits tomato Rcr3 protease required for
1001 *Cf-2*-dependent disease resistance. *Science* **308**: 1783–1786.

1002 **Rouxel T, Grandaubert J, Hane JK, Hoede C, van de Wouw AP, Couloux A,**
1003 **Dominguez V, Anthouard V, Bally P, Bourras S, *et al.* 2011**. Effector diversification
1004 within compartments of the *Leptosphaeria maculans* genome affected by
1005 repeat-Induced point mutations. *Nature Communications* **2**: 202.

1006 **Sainsbury F, Thuenemann EC, Lomonossoff GP**. **2009**. pEAQ: versatile expression
1007 vectors for easy and quick transient expression of heterologous proteins in plants. *Plant*
1008 *Biotechnology Journal* **7**: 682–693.

1009 **Sanderson MJ**. **2003**. r8s: inferring absolute rates of molecular evolution and
1010 divergence times in the absence of a molecular clock. *Bioinformatics* **19**: 301–302.

1011 **Shahid S, Kim G, Johnson NR, Wafula E, Wang F, Coruh C, Bernal-Galeano V,**
1012 **Phifer T, dePamphilis CW, Westwood JH, *et al.* 2018**. MicroRNAs from the parasitic
1013 plant *Cuscuta campestris* target host messenger RNAs. *Nature* **553**: 82–85.

1014 **Snelders NC, Kettles GJ, Rudd JJ, Thomma BPHJ**. **2018**. Plant pathogen effector
1015 proteins as manipulators of host microbiomes? *Molecular Plant Pathology* **19**:
1016 257–259.

1017 **Song W-Y, Wang G-L, Chen L-L, Kim H-S, Pi L-Y, Holsten T, Gardner J, Wang**
1018 **B, Zhai W-X, Zhu L-H, *et al.* 1995**. A receptor kinase-like protein encoded by the rice
1019 disease resistance gene, *Xa21*. *Science* **270**: 1804–1806.

Spanu PD, Abbott JC, Amselem J, Burgis TA, Soanes DM, Stüber K, Themaat EVL van, Brown JKM, Butcher SA, Gurr SJ, *et al.* 2010. Genome expansion and gene loss in powdery mildew fungi reveal tradeoffs in extreme parasitism. *Science* **330**: 1543–1546.

Stamatakis A. **2006**. RAxML-VI-HPC: maximum likelihood-based phylogenetic analyses with thousands of taxa and mixed models. *Bioinformatics* **22**: 2688–2690.

Takahara H, Dolf A, Endl E, O'Connell R. **2009**. Flow cytometric purification of *Colletotrichum higginsianum* biotrophic hyphae from Arabidopsis leaves for stage-specific transcriptome analysis. *The Plant Journal* **59**: 672–683.

Takeuchi O, Akira S. **2010**. Pattern recognition receptors and inflammation. *Cell* **140**: 805–820.

Tang D, Wang G, Zhou J-M. **2017**. Receptor kinases in plant-pathogen interactions: more than pattern recognition. *The Plant Cell* **29**: 618–637.

Tisserant E, Malbreil M, Kuo A, Kohler A, Symeonidi A, Balestrini R, Charron P, Duensing N, Frei dit Frey N, Gianinazzi-Pearson V, *et al.* 2013. Genome of an arbuscular mycorrhizal fungus provides insight into the oldest plant symbiosis. *Proceedings of the National Academy of Sciences, USA* **110**: 20117–20122.

Torres MA, Jones JDG, Dangl JL. **2006**. Reactive oxygen species signaling in response to pathogens. *Plant Physiology* **141**: 373–378.

Tsushima A, Gan P, Kumakura N, Narusaka M, Takano Y, Narusaka Y, Shirasu K. **2019**. Genomic plasticity mediated by transposable elements in the plant pathogenic fungus *Colletotrichum higginsianum*. *Genome Biology and Evolution* **11**: 1487–1500.

Tsushima A, Narusaka M, Gan P, Kumakura N, Hiroyama R, Kato N, Takahashi S, Takano Y, Narusaka Y, Shirasu K. **2021**. The conserved *Colletotrichum* spp. effector candidate CEC3 induces nuclear expansion and cell death in plants. *Frontiers in Microbiology* **12**: 2535.

Wan J, Zhang X-C, Neece D, Ramonell KM, Clough S, Kim S, Stacey MG, Stacey G. **2008**. A LysM receptor-like kinase plays a critical role in chitin signaling and fungal resistance in *Arabidopsis*. *The Plant Cell* **20**: 471–481.

Wang M, Weiberg A, Lin F-M, Thomma BPHJ, Huang H-D, Jin H. **2016**. Bidirectional cross-kingdom RNAi and fungal uptake of external RNAs confer plant protection. *Nature Plants* **2**: 16151.

Weiberg A, Wang M, Lin F-M, Zhao H, Zhang Z, Kaloshian I, Huang H-D, Jin H. **2013**. Fungal small RNAs suppress plant immunity by hijacking host RNA interference pathways. *Science* **342**: 118–123.

Win J, Chaparro-Garcia A, Belhaj K, Saunders DGO, Yoshida K, Dong S, Schornack S, Zipfel C, Robatzek S, Hogenhout SA, *et al.* 2012. Effector biology of plant-associated organisms: concepts and perspectives. *Cold Spring Harbor Symposia on Quantitative Biology* **77**: 235–247.

Wymelenberg AJ vanden, Cullen D, Spear RN, Schoenike B, Andrews JH. **1997**. Expression of green fluorescent protein in *Aureobasidium pullulans* and quantification of the fungus on leaf surfaces. *Biotechniques* **23**: 686–690.

35

1062 **Yang J, Wang L, Ji X, Feng Y, Li X, Zou C, Xu J, Ren Y, Mi Q, Wu J, *et al.* 2011**.
1063 Genomic and proteomic analyses of the fungus *Arthrobotrys oligospora* provide
1064 insights into nematode-trap formation. *PLOS Pathogens* **7**: e1002179.

1065 **Yoshino K, Irieda H, Sugimoto F, Yoshioka H, Okuno T, Takano Y**. **2012**. Cell
1066 death of *Nicotiana benthamiana* is induced by secreted protein NIS1 of *Colletotrichum*
1067 *orbiculare* and is suppressed by a homologue of CgDN3. *Molecular Plant-Microbe*
1068 *Interactions* **25**: 625–636.

1069 **Zampounis A, Pigné S, Dallery J-F, Wittenberg AHJ, Zhou S, Schwartz DC, Thon**
1070 **MR, O'Connell RJ**. **2016**. Genome sequence and annotation of *Colletotrichum*
1071 *higginsianum*, a causal agent of crucifer anthracnose disease. *Genome Announcements*
1072 **4**: e00821-16.

1073 **Zhang T, Zhao Y-L, Zhao J-H, Wang S, Jin Y, Chen Z-Q, Fang Y-Y, Hua C-L,**
1074 **Ding S-W, Guo H-S**. **2016**. Cotton plants export microRNAs to inhibit virulence gene
1075 expression in a fungal pathogen. *Nature Plants* **2**: 16153.

1076

Supporting Information

1078 Figure S1. Alignment of *C. orbiculare* SRNs

1079 Figure S2. SRNs expressed in *N. benthamiana* with the pEAQ binary vector

1080 Figure S3. Establishment of the *Agrobacterium*-mediated transient gene expression system in *C. sativus*

1082 Figure S4. Oxidative bursts are elicited by chitin on *C. sativus* cotyledons

1083 Figure S5. The two predicted glycosylation sites in SRN2 are not involved in the potentiation of chitin-triggered ROS bursts

1085 Figure S6. Assessment of PTI marker gene candidates in *C. sativus*

1086 Figure S7. SRN1 does not cleave dsRNAs

1087 Figure S8. Phenotype of *N. benthamiana* expressing SRN2 mutant proteins

1088 Table S1. List of *Colletotorichum orbiculare* conserved effector candidates

1089 Table S2. List of 32 fungal genomes

1090 Table S3. Plasmid list

1091 Table S4. DNA oligonucleotide list

1092 Table S5. Fungal strain list

1093 Table S6. Accession numbers of *SRN* genes

1094 Table S7. Number of *SRN* genes in *Colletotrichum* species

1095 Method S1. Plasmid construction

1096 Method S2. Fungal transformation

1097 Method S3. Fungal inoculation

1098   Method S4. Immunoblotting

1099   Method S5. Recombinant protein expression and purification

1100   Method S6. Linker ligation of RNAs